NON-LINEAR CONTROL SYSTEMS

SOME ASPECTS

ON

NON-LINEAR CONTROL SYSTEMS

By

AKIRA ITO, B.E.

A Thesis

Submitted to the Faculty of Graduate Studies

in Partial Fulfilment of the Requirements

for the Degree

Master of Engineering

McMaster University

May 1965

MASTER OF ENGINEERING(1965) (Electrical Engineering)

McMASTER UNIVERSITY Hamilton, Ontario.

TITLE: Some Aspects on Non-Linear Control Systems

AUTHOR: Akira Ito, B.Eng. (The University of Osaka Pref., Japan)

SUPERVISOR: Proffessor D. P. Atherton

NUMBER OF PAGES: vi, 66

SCOPEAND CONTENTS: The thesis consists of two parts. In part I, A brief description of an analog computer constructed for the non-linear simulation is given. In part II, a new approach to examine the behavior of feedback systems with relay type non-linear characteristics is discussed: a harmonic analysis of the sustained oscillation in the systems was carried out, and the results were verified experimentally.

PREFACE

It is said there is no general approach to examine the behavior of the non-linear control systems. Every technique developed in the field of the non-linear control engineering has a limited area of application. Therefore, every technique must be accumulated so that the technology will be formed more systematically and perfectly.

In this work several topics were selected, however, the emphasis was on the study of the nature of relays which today offer diverse field of application to the industry as economical and efficient devices for automatic control.

ACKNOWLEDGMENTS

The author wishs to express sincere thanks to his supervisor, Dr. D. P. Atherton, for his guidance toward the completion of this research work. The author is also thankful to Dr. A. S. Gladwin, chairman of the Electrical Engineering department, for his encouragement and help.

TABLE OF CONTENTS

LIST OF PRINCIPAL SYMBOLS

e_o = instantaneous value of output signal from a non-linear characteristic

e_i = instantaneous value of input signal to a non-linear characteristic

r_o = d.c. component of output signal from a non-linear characteristic

r_i = d.c. component of input signal to a non-linear characteristic

r = d.c. component of input signal to a feedback system

c = instantaneous value of output signal of a feedback system

$G(s)$ = transfer function of a linear system

n = positive integer

ω = angular frequency

T = time constant

λ = normalized angular frequency = ωT

K = linear gain of a system

h = saturation level of a non-linear characteristic

2δ = hysteresis width or dead-zone of a non-linear characteristic

β = switching angle of a periodic waveform

a_n = Fourier coefficient of a periodic function

D = (sinusoidal) describing function

C = critical locus function = $-1/D$

Part I ANALOG COMPUTER

1 General Description

An analog computer with 20 unit amplifiers and several types of non-linear characteristic has been constructed. The computer was required for high speed simulation of non-linear feedback control systems. Techniques to simulate certain non-linearities have been studied and several types were developed. These include saturation, dead-zone, back-lash, on-off with dead-zone and a pure on-off characteristic.

The computer contains 20 linear amplifiers (4 of which are chopper stabilized), a total number of twelve non-linear characteristics, one dual beam oscilloscope and a power supply. All elements are assembled on the back side of rack mounted panels. Jacks are arranged on the panels to achieve flexible inter-connections between the input and output elements. The panels, oscilloscope and power supply are all mounted on a rack as shown in the photograph, fig. 1.

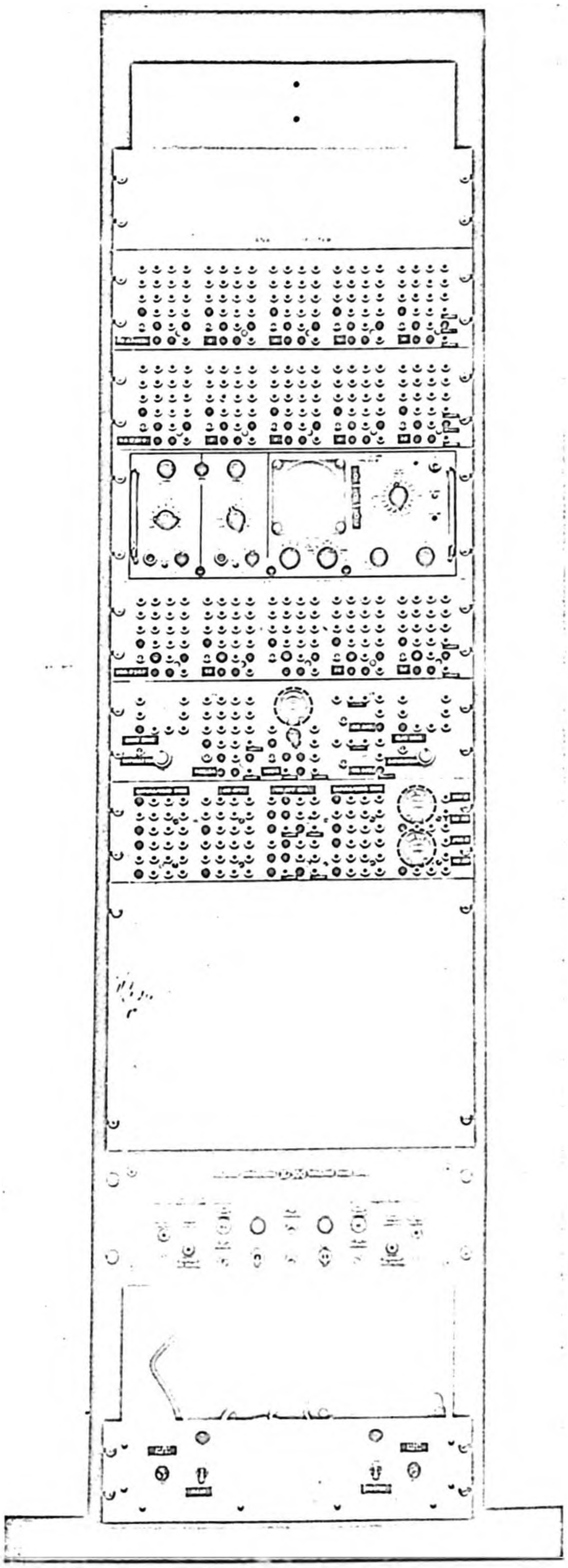

Fig. 1

Analog

Computer

2. Components

2.1. Operational Amplifiers

Three kinds of operational amplifiers are used in this computer, Philbrick Researches Inc. types K2-W, K2-XA and USA-3. The K2-W is an octal based plug-in type unit containing two twin triodes 12AX7 which are housed in a molded plastic case. It has a nominal gain of 15,000, a response time of 2 micro-second and an output current of 1mA. The K2-XA is an improved version of the K2-W with increased gain, response and output power. A summary of the maker's specifications for the K2-W and K2-XA is shown in table 1. Fig. 3 shows typical examples of static input-output characteristics of unit amplifiers, K2-W and K2-XA. Fig. 4 shows the frequency response of the K2-W. For use as integrators, four stabilized amplifiers, Philbrick model USA-3, are provided. The gain-frequency curve of this amplifier has a 6db/octave fall off from a gain of 10^8 at 0.01c/s, giving unity gain in the region of 1 magacycle.

	K2-W	K2-XA
Open loop gain (dc)	15,000	30,000
Rise time (as an unity gain inverter)	2μsec	1μsec
Drift rate (refered to the input)	+5mv/day	+8mv/day
Input impedance	above 100meg and 7μμf	100meg and 7μμf
Output impedance	below 1kΩ	below 1kΩ
Output current(max) at output voltage	±1.0ma ±50v	+6.1, -2.8ma +100v

Table 1 Specification of K2-W and K2-XA (summary)

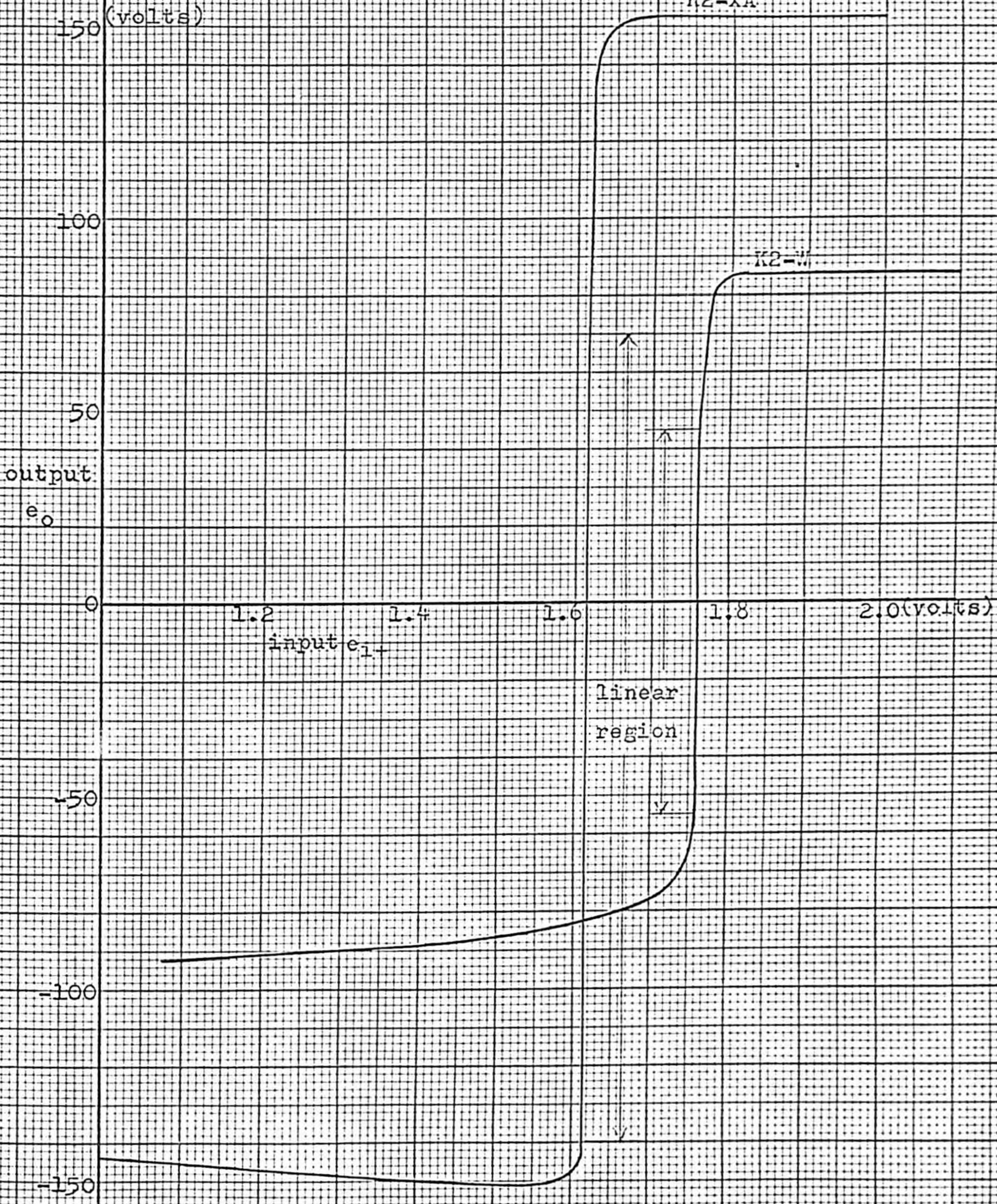

Fig. 3   Input-output characteristics of operational amplifiers
(negative input terminal grounded, no zero compensation)

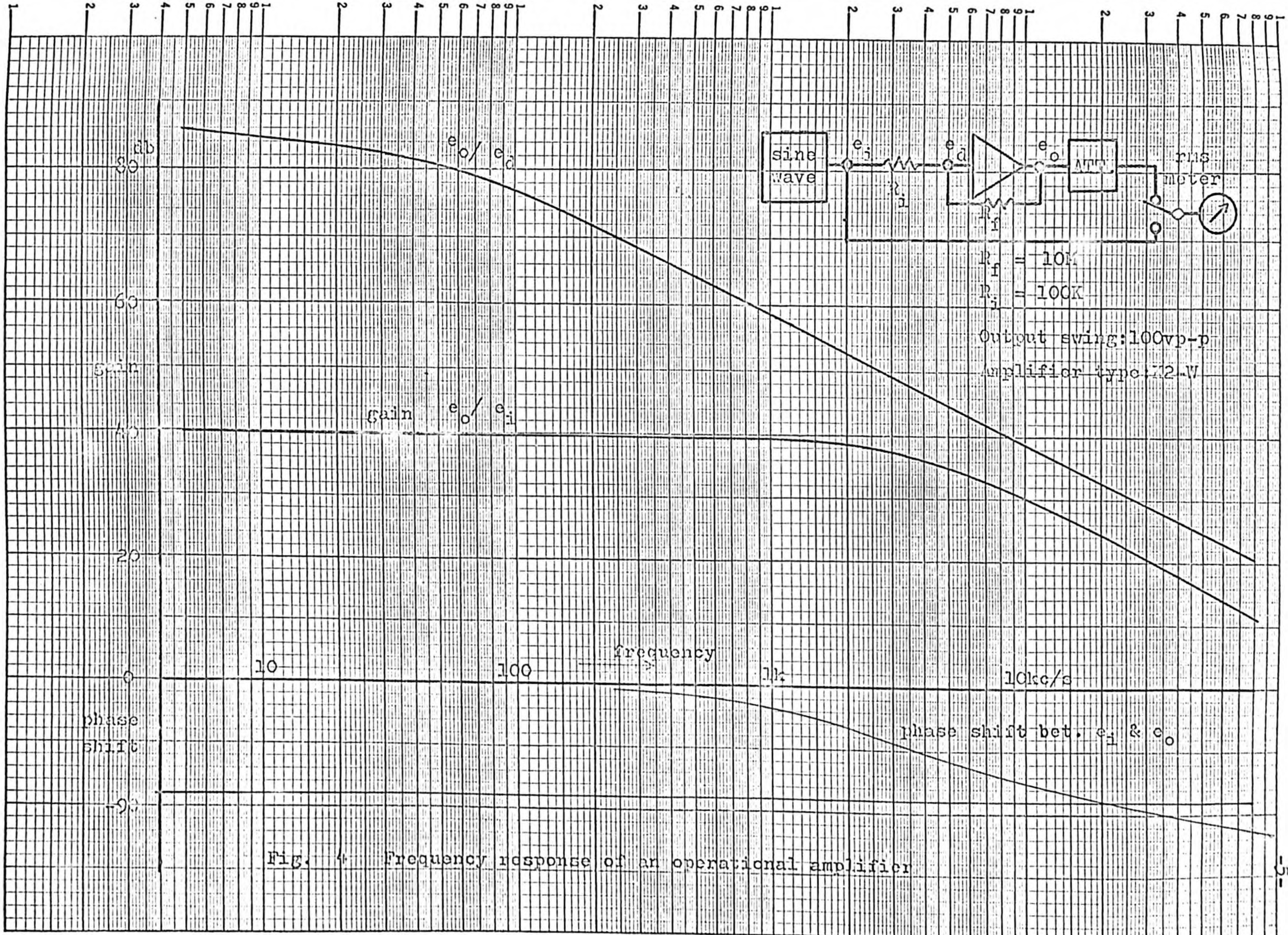

Fig. 4 Frequency response of an operational amplifier

2.2 Power Supply

2.2.1 High Voltage Supply

A Philbrick model R-300 regulated power supply was used to provide outputs of +300 and -300volts dc with a maximum of 300 milliamps load current. The regulation, stability and transient regulation of the power supply were checked and results were found to be satisfactory. The summarized maker's specification is shown in table 2.

Output current		0 - 300ma rated max. at +300vdc 0 - 300ma rated max. at -300vdc
Input		105 - 125vdc, 50 - 60c/s
Stability		+100mv over a 24hour period
Noise		250 microvolts acrms
Transient regulation		Under 3 mvdc (0.001%)
Internal impedance	0 - 10kc	under 0.01 ohm
	above 10kc	a shunt capacitor of 150uf whose series r is 0.2 ohm

Table 2 Specification of R-300 power supply

2.2.2 Heater Voltage Supply

In order to reduce drift in the unstabilized amplifiers, a magnetic type filament voltage regulator was used. The regulator has an output voltage of 6.3volts $\pm$ 0.1% with a maximum load current of 25amps at 60c/s.

2.3. Non-Linear Characteristics

2.3.1 Saturation and Dead-Zone

There are several methods for obtaining these characteristics suggested in the literature.[(1),(2),(3)] Every one of them, however, is generally unsatisfactory because of a lack of sharpness at the corners of the input-output characteristic, the introduction of hysteresis at relatively low frequencies, or the circuitry requires several unit amplifiers. Fig. 7 shows one type of saturation characteristic tested and used in the computer, which requires 6 diodes and no auxliary amplifier. The input-output characteristic gives reasonably sharp and symmetrical corners. One extra advantage of the circuit is that it can easily be converted to a dead-zone characteristic with the addition of an adding amplifier and a slight change of connections. The combined circuit for the saturation and dead-zone characteristic is shown in fig. 8. The photographs in fig. 9 show the input-output characteristics obtained at a frequency of 200c/s. On the computer panel there are six elements for these combined characteristics, two of them with adjustable clipping levels.

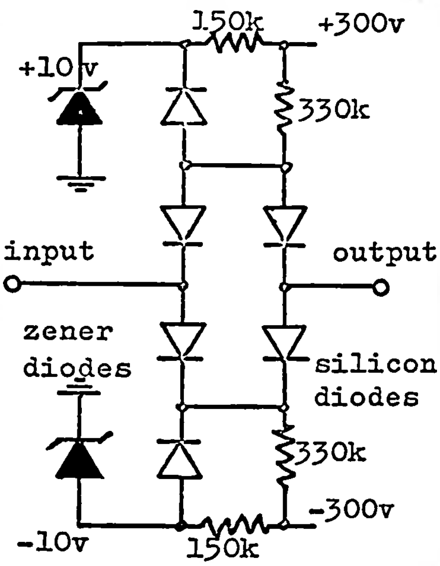

Fig. 7 Circuit for saturation characteristic

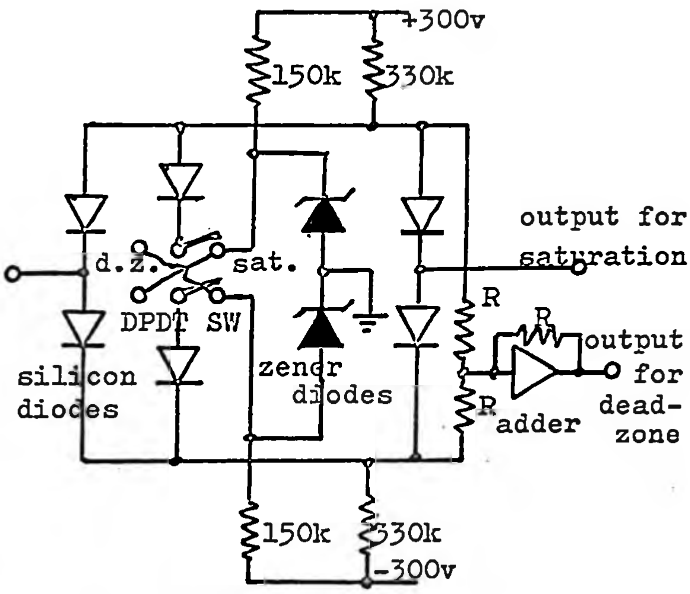

Fig. 8 Combined curcuit for saturation and dead-zone

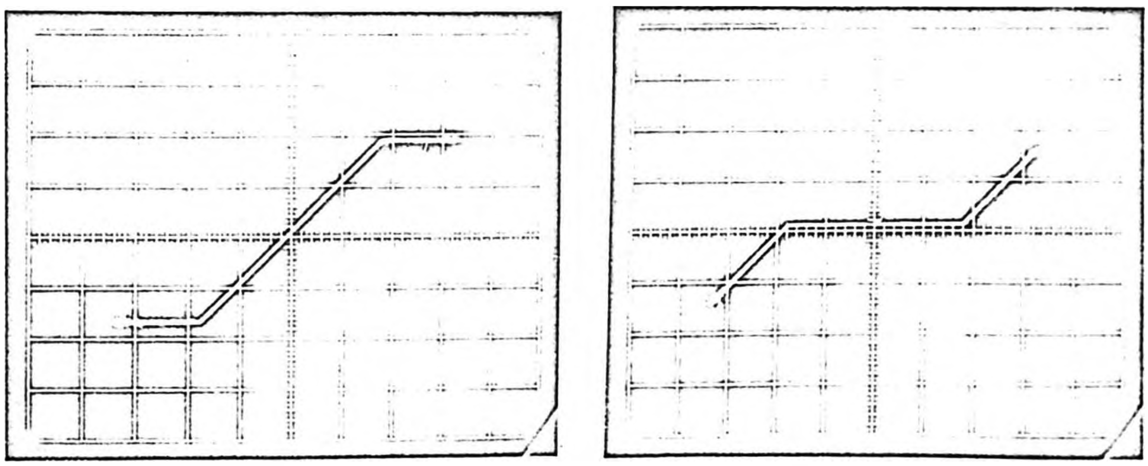

Fig. 9 Input-output characteristics of saturation and dead-zone (horizontal and vertical scale: 5v/division)

2.3.2 On-Off with Hysyeresis

The circuit[3] shown in fig.10 was tried, and the part enclosed by a broken line was made as a plug-in unit which is shown in fig. 12. Because the output of the stage did not have square edges, a saturation element had to follow it to reshape the waveform. The hysteresis width of this circuit varies considerably as the input amplitude varies. This variation was about 10% when the peak amplitude changes from 100% to 500% of the hysteresis width.

To get a more stable hysteresis width and a faster response, the Schmidt trigger circuit[4] shown in fig. 11 was tested and gave satisfactory results. The photographs in fig. 13 show the input-output characteristics of the circuit at several frequencies and amplitudes. Two of these circuits were built on the computer panel.

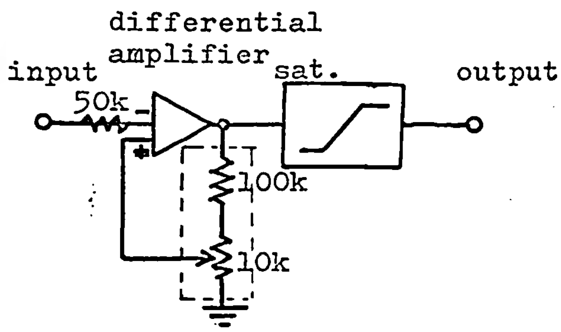

Fig.10 On-off with hysteresis circuit (positive feed-back type)

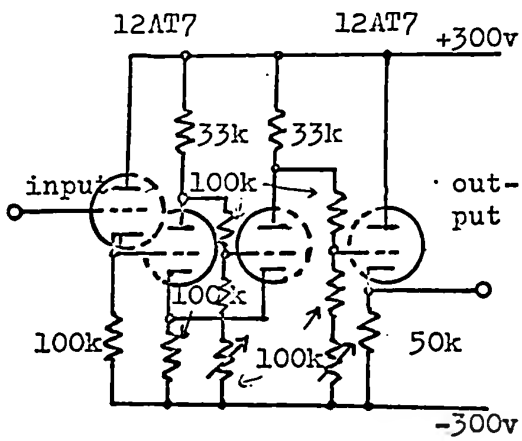

Fig.11 On-off with hysteresis (Schmidt trigger)

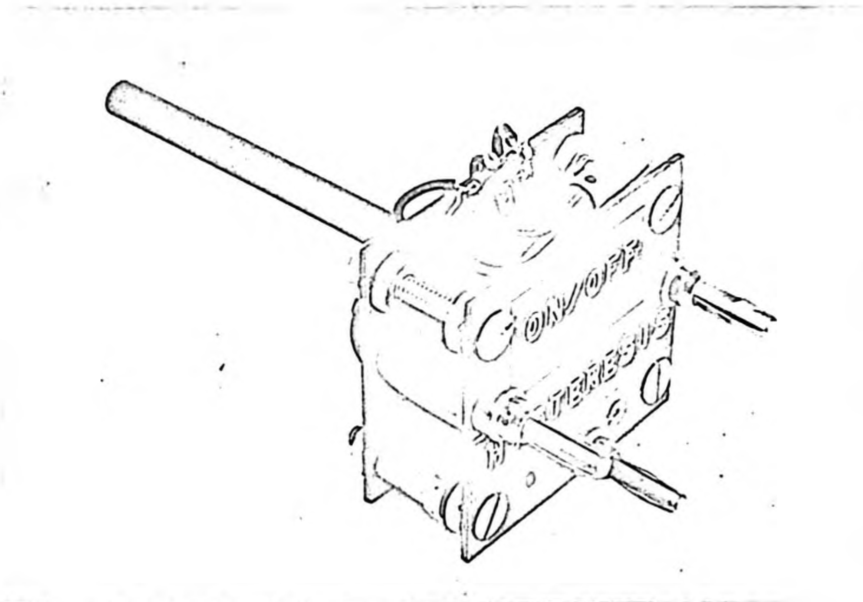

Fig. 12 A plug-in unit for on-off with hysteresis

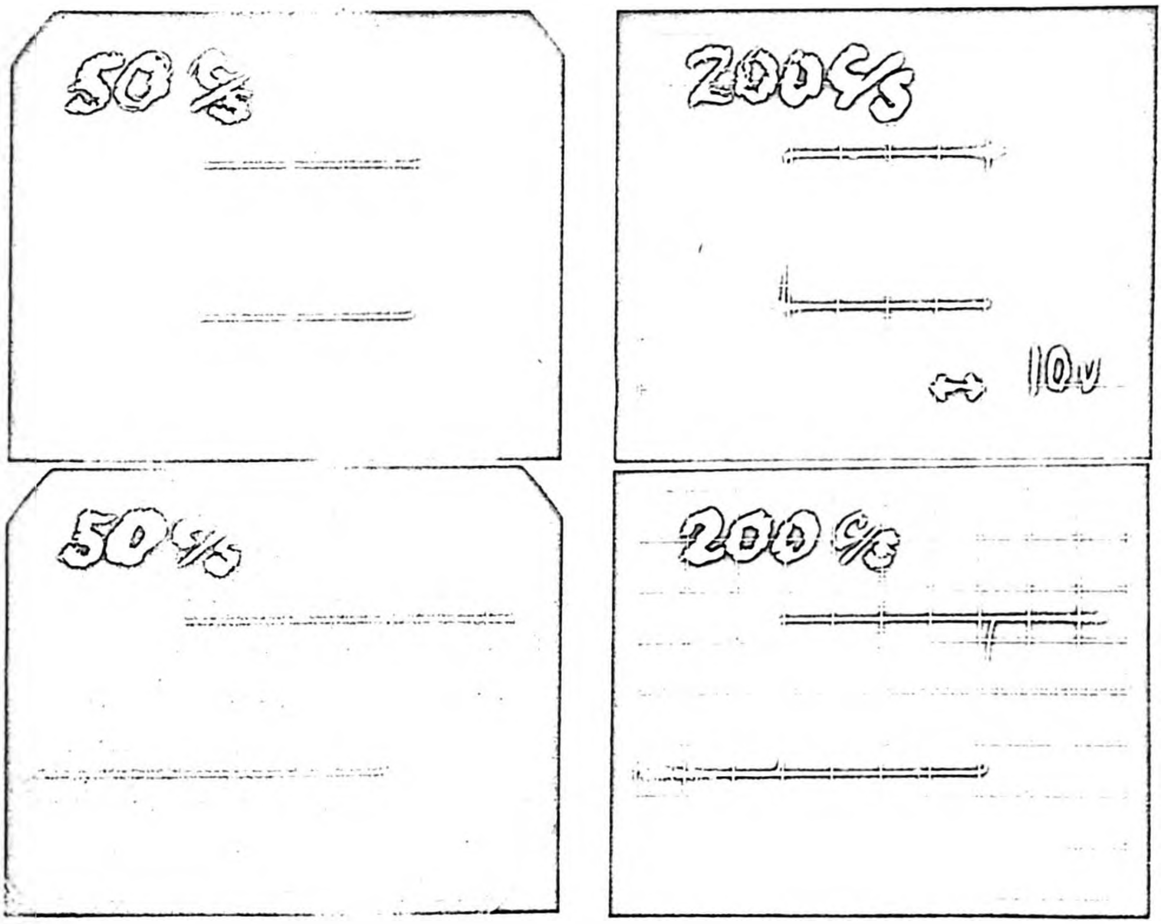

Fig. 13 Input-output characteristics of the on-off with hysteresis (Schmidt trigger) circuit
(vertical and horizontal scale: 10v/div.)

2.3.3 On-off and on-off with dead-zone

The circuit for a pure on-off characteristic is shown in fig. 14. Two of these circuits were built on the panel. The zener diode which determines the output height is connected externally to the terminals provided.

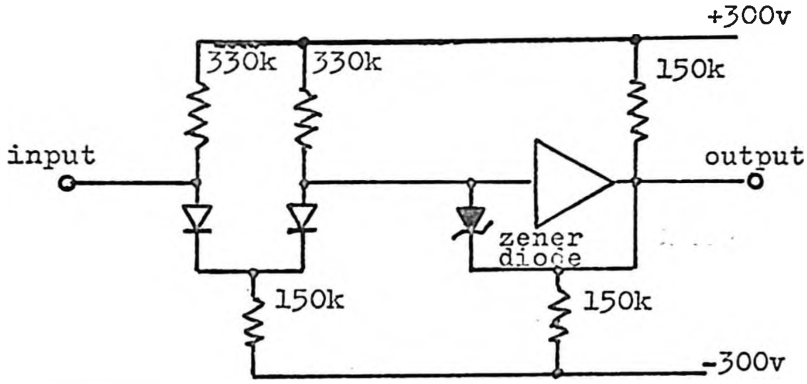

Fig.14. Circuit for on-off characteristic

The on-off with dead-zone characteristic can be obtained by adding the outputs of the two on-off elements whose operating input voltages are separated by the value of the dead-zone. Fig. 15(a) shows the schematic diagram for this and (b) the resultant input-output characteristic.

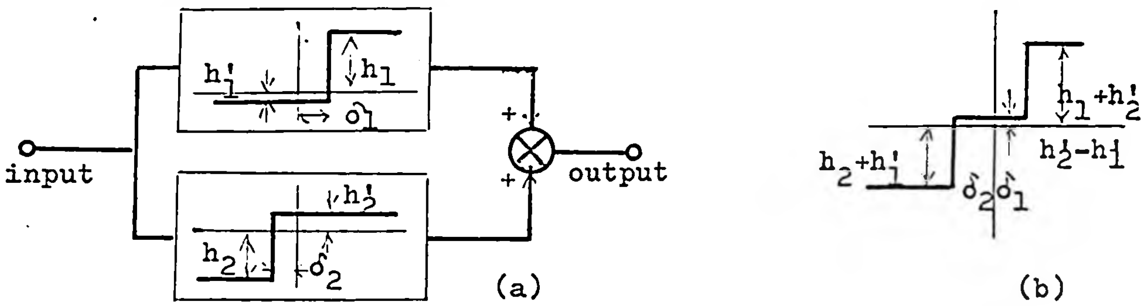

Fig.15 Adding of two on-off characteristics

2.3.4 Back lash

This element can be constructed using a dead-zone characteristic as shown in fig. 16. The circuit has a certain frequency limit for accurate operation. In practice, the input frequency should be less than K/100T for good result.

Fig. 17 shows another circuit for this characteristic. The circuit is relatively simple but requires a high input impedance voltage follower. This non-linear element was prepared as a plug-in attachment, as shown in the photograph in fig. 18. It can be used with any unit amplifier on the panel.

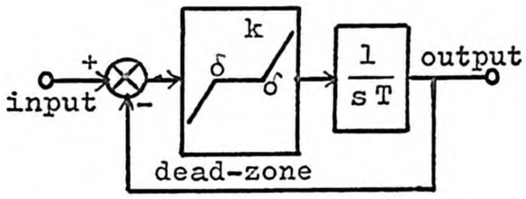

Fig. 16 A circuit for backlash

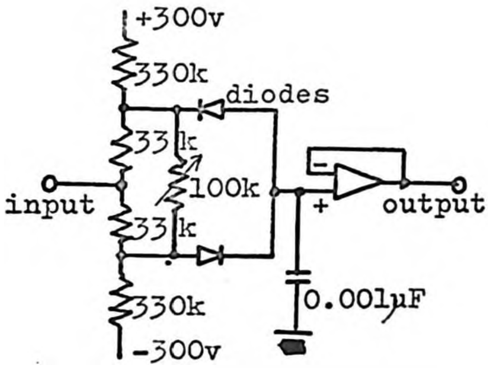

Fig. 17 A circuit for backlash

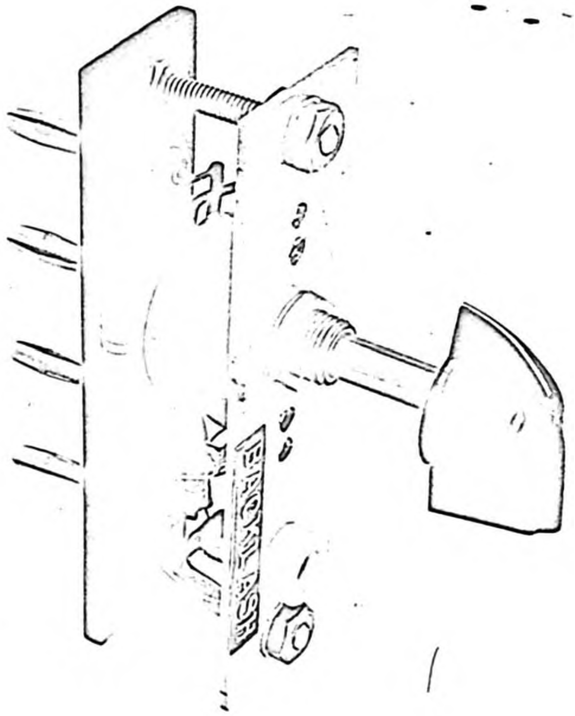

Fig. 18 Plug-in attachment for backlash

2.4 Variable Gain Amplifier

The combination of a potentiometer and a fixed gain amplifier can be used to give a variable gain amplifier. But the variable feedback ratio type is preferable to keep a low signal-to noise ratio and a large output level at any setting of the gain. The two types of circuit, shown in fig. 20, were chosen. The type (a) gives a gain of 1 to 10 on the high gain range and 0.1 to 1 on the low gain range. The gain of the type (b) circuit can be set to any ratio by putting R_1 and R_2 externally to the terminal provided. Theis type gives good linearity when the gain range used is small. (For example, when R_1, R_2 and R are all 100k giving a -6db to 6db range, see fig. 21 curve I.) Fig. 21 shows the calibration curves of the variable gain amplifiers.

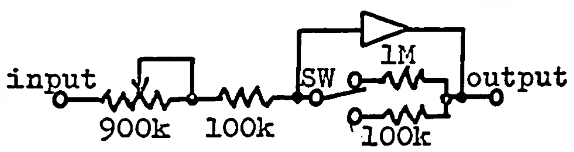

(a) VGA I

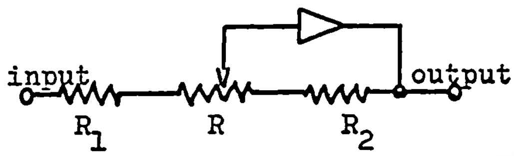

(b) VGA II and VGA III

Fig. 20 Variable gain amplifiers

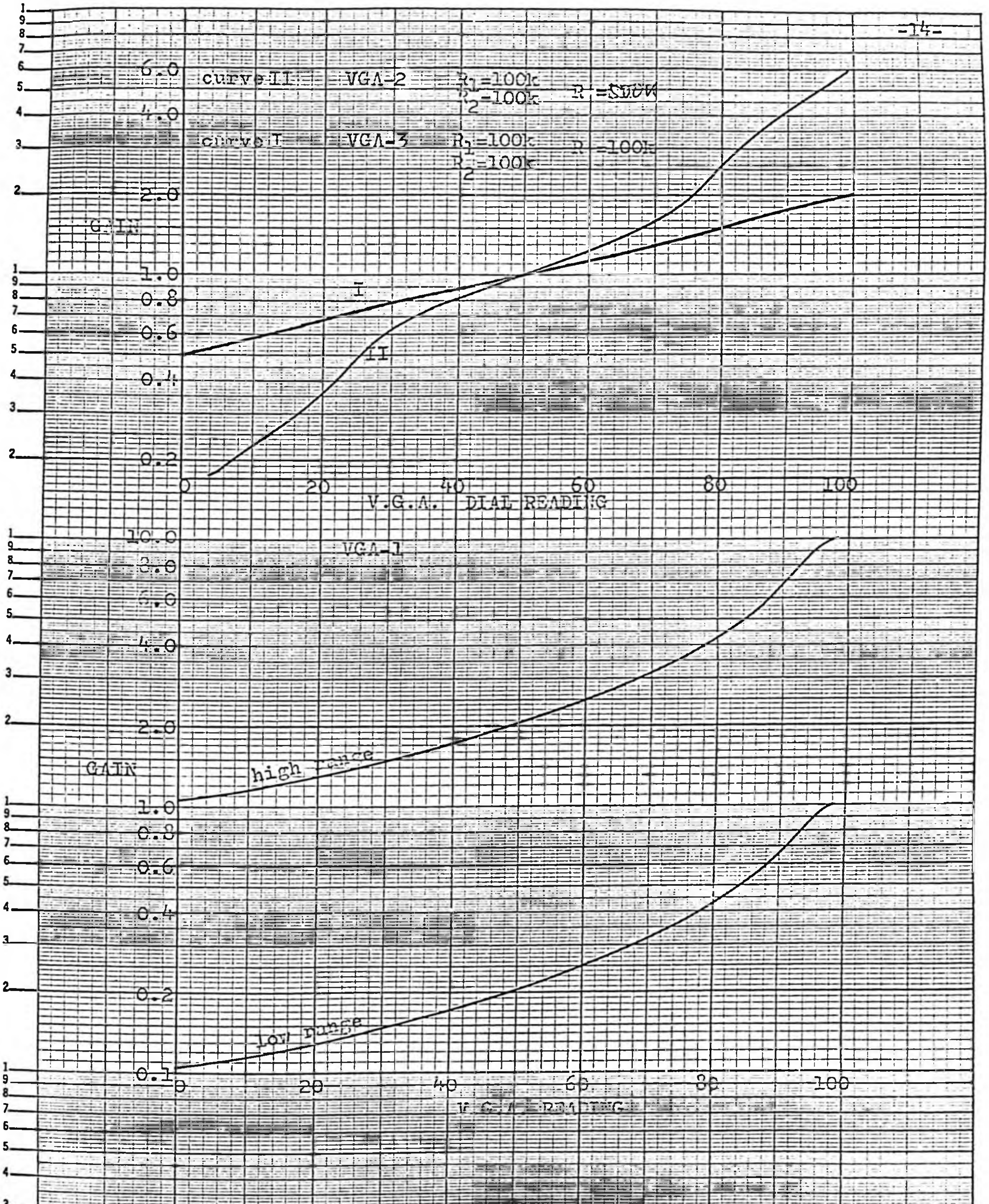

Fig. 21 Calibration curve of Variable Gain Amplifiers

2.5. Noise Generator

Fig. 22 shows a circuit diagram tested in an experimental set up. The noise is generated in a Sylvania gas filled 6D4 tube. A cylindrical magnet around the tube is used to get a maximum output noise. The effect of the magnet can be explained as follows; if a magnetic flux is applied passing parallel to the axis of the cylindrical electrode, the path of the electrons is bent to a spiral trajectory thus increasing the probability of electron ion collisions, thus the increased number of ions per unit time arriving at the cathode provides a bigger noise. The measured output voltage of the circuit is 1.05v rms. The cutoff frequencies of the amplifier (3db points) are 16c/s at the low frequency side and 3.2kc/s at the high side. The frequency spectrum of the noise is observed to be reasonably flat between the cutoff frequencies.

It was found that in ordinary use, the induced 60 cycle hum in the output could not be suppressed to a reasonably low level unless the 6D4 heater was supplied from a d.c. source. The photographs in fig.23 show the output waveforms of the noise after passing through the very narrow bandpass filter with a center frequency of 80c/s (see fig. A for the circuit and its response). The waveform (a) is from the noise generator with a.c. heater supply and (b) with d.c. The former clearly shows the existence of the 60 cycle voltage since the time base of the oscilloscope was triggered by the line voltage.

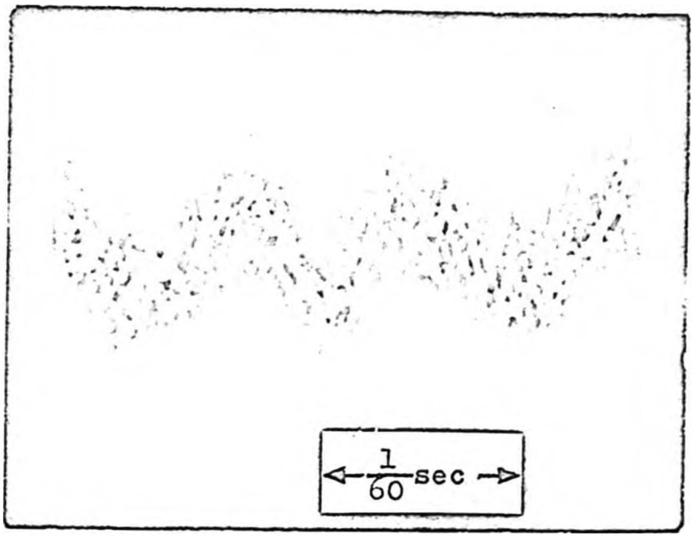

Fig. 23 (a) Random noise containing 60 cycle hum
(6D4 heater: 6.3volts a.c.)

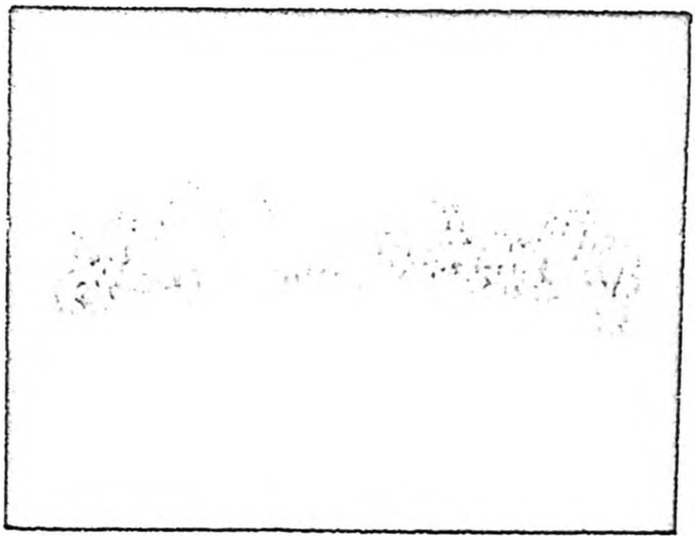

Fig. 23 (b) Random noise
(6D4 heater: 6.3volts d.c.)

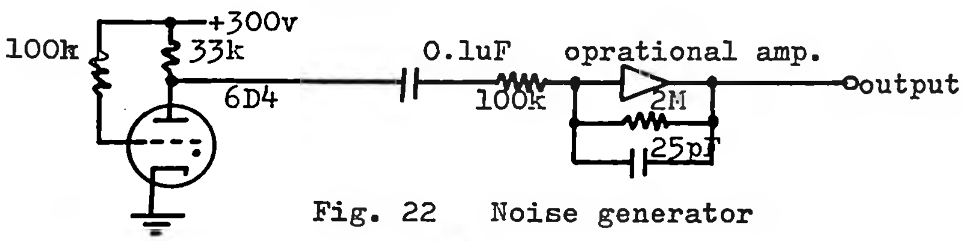

Fig. 22 Noise generator

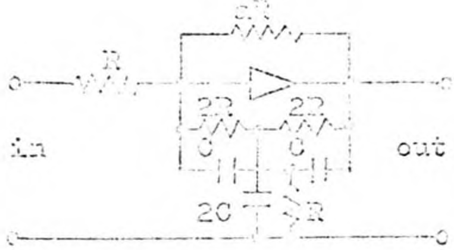

$R=100k$

$C=0.001\mu F$

$a=100$

$T=RC=0.0001sec$

$f_0=1/4\pi T \cong 80c/s$

$gain=100$

Fig. A (a) Circuit for the band-pass filter

Fig. A (b) Frequency response of the band-pass filter

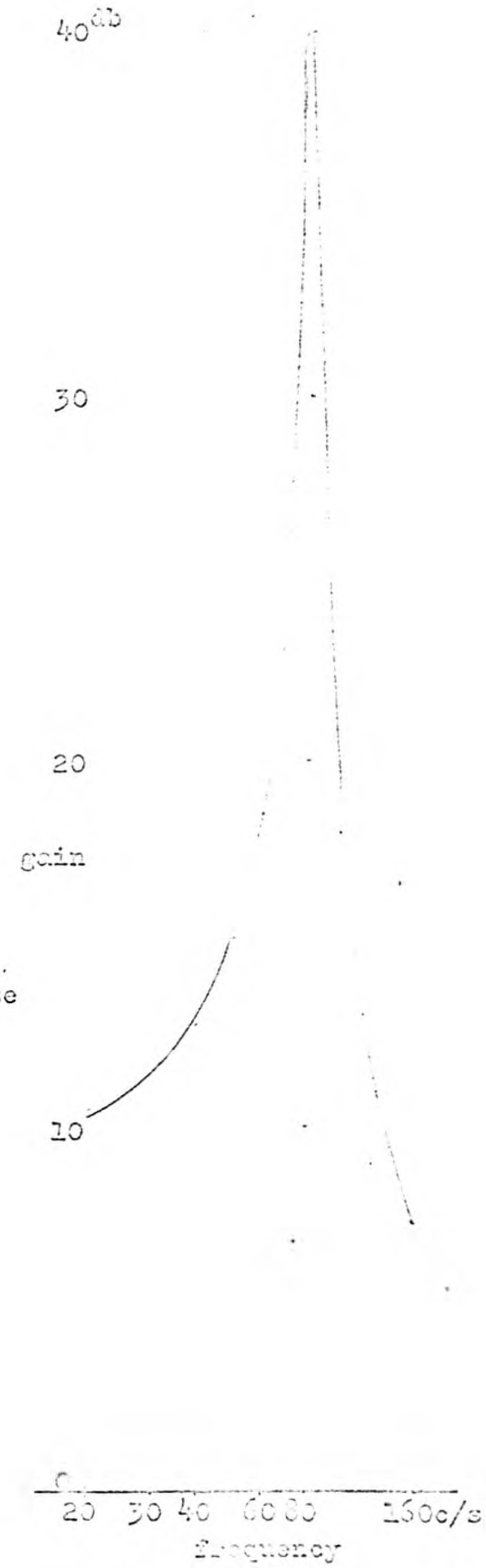

Summary of Part II

The behaviour of feedback systems with relay type non-linear characteristics is discussed. The basic form of the system studied is shown in fig. 24 on page 20.

For the pruposes of the analysis it is assumed that the output $e_o(t)$ of the non-linear element has a specified periodic wave-shape, but with certain undetermined coefficients. The input to the non-linear elment is calculated from this in the form of a Fourier series. Equating the values of this input at the assigned switching instants to the value required by the non-linear characteristic yields a set of equations through which the undetermined coefficients mentioned above are determined.

The solution to these equations is obtained by the developement of a 'critical response locus' method. The modified frequency response locus as an intermediate step in the solution is derived from an infinite summation but closed analytic solutions are developed for some of the situations discussed.

Examples are presented in which the method is applied to three different types of non-linear characteristic. Experimental results are compared with values predicted by analysis.

Although the emphasis is on finding the frequency of oscillation, the evaluation of the signal at any point in the system is also desirable.

Part II . MODIFIED FREQUENCY RESPONSE LOCUS TECHNIQUE FOR SYSTEMS CONTAINING A NON-LINEAR ELEMENT

1 Introduction

1.1 Detail of type of system investigated

This study seeks to predict the oscillation frequency of systems of the type indicated in fig. 24 for various non-linear transfer characteristics. There already exist two methods, namely (a) the phase plane method and (b) the describing function method, for the development of such predictions. The phase plane method is restricted to systems for which the linear transfer function G(s) is of order 2 or less, while the describing function technique requires that G(s) shall have a lowpass characteristic.

The modified frequency locus concept here studied was proposed by Atherton and is similar to methods suggested earlier by Tsypkin.(5),(6)

1.2 Types of Non-Linearity

The types of non-linear characteristic studied here are on-off, on-off with hysteresis, on-off with dead-zone, and saturation, and shown if fig. 25 (a), (b), (c) and (d).

2 Theory of the Modified Frequency Response Method

2.1 Approach

It is assumed that the non-linear control system consists of two parts. One is a linear portion which can be described as a transfer function. The other is a single or double valued non-linear characteristic. Fig. 24 shows the schematic diagram of such a non-linear system. If the input and output of the non-linear element have periodic waveforms, they can be represented by a Fourier series expression. Let the output of the non-linearity e_o be

$$e_o = r_o + \sum_{n=1}^{\infty} a_n \cos n\omega t \;{}^{*} \qquad 101$$

where r_o is a d.c. component and a_n's are coefficients of a Fourier series. The output of the system, c, is given by

$$c = r_o G(0) + \sum_{n=1}^{\infty} a_n G_n \cos(n\omega t - \varphi_n) \qquad 102$$

where G_n and φ_n are the gain and phase lag respectively of G(s) (the linear portion of the system) at the angular frequency $n\omega$.
If the system has a d.c. input signal, the input signal e_i to the non-linearity is the difference of r and c, and may be expressed by

$$e_i = r_i - \sum_{n=1}^{\infty} a_n G_n \cos(n\omega t - \varphi_n) \qquad 103$$

Where r_i is the d.c. component at the input of the non-linearity.

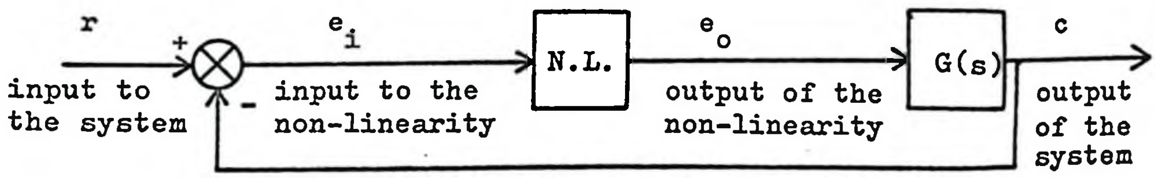

Fig. 24 Non-linear control system

* In some non-linear systems with closed loop, this assumption is possible (without giving much error) by proper selection of the time origin.

Further study depends on the type of non-linear characteristic and the switching condition which will be discussed in next section. The non-linear characteristics considered here are limited to the following types, on-off, on-off with hysteresis, on-off with dead-zone, on-off with dead-zone and hysteresis, saturation and dead-zone, and are shown in fig. 25.

A pure on-off characteristics may be considered as a specific case of on-off with hysteresis or on-off with dead-zone, where the hysteresis width or dead-zone are respectively zero. Also it can be considered a specific case of saturation where the gain of the linear portion of the characteristic tends to infinity.

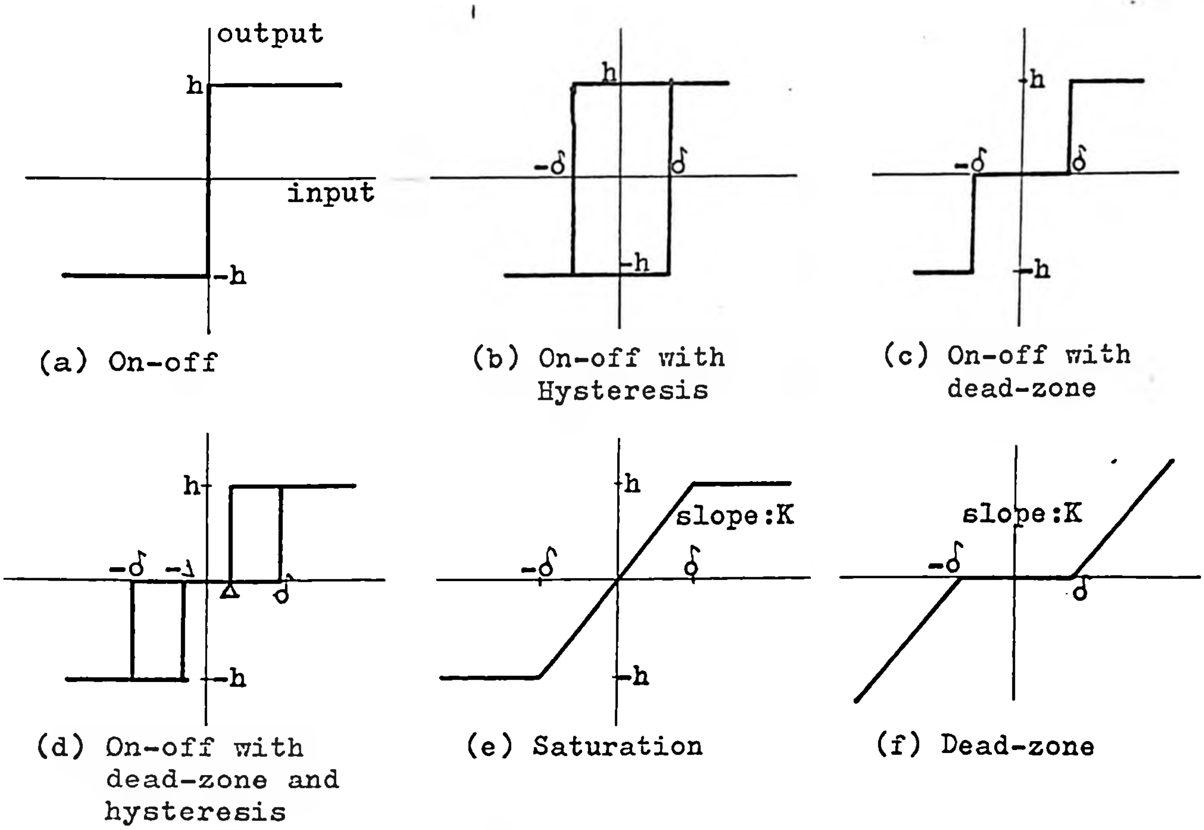

(a) On-off

(b) On-off with Hysteresis

(c) On-off with dead-zone

(d) On-off with dead-zone and hysteresis

(e) Saturation

(f) Dead-zone

Fig.25 Non-linear characteristics

2.2. Switching Condition

The output waveforms from those non-linear characteristics under consideration consist of several flat lines which are the saturation levels or dead-zone levels and, for a given frequency, are independent of time, together with sections which are proportional to the input waveforms. The times when the waveform goes into and comes out of the saturation level or dead-zone level are considered to be switching instants. In the non-linear system, there are two switching instants in case of an on-off with hysteresis characteristic and four in other cases.

2.3. Case for Two- Switching Condition

The input and output waveforms of on-off with hysteresis are shown in fig. 26. If the time origin is taken as shown in the figure, the switching instants can be taken at times $t_1 = -\beta/\omega$ and $t_2 = \beta/\omega$. Assuming the corresponding values of input e_i at the instants are ψ_1 and ψ_2, then from eqn.103 we have the relationship

$$\psi_1 = r_i - \sum_{n=1}^{\infty} a_n G_n \cos(-n\beta - \varphi_n) \qquad 104$$

$$\psi_2 = r_i - \sum_{n=1}^{\infty} a_n G_n \cos(n\beta - \varphi_n) \qquad 105$$

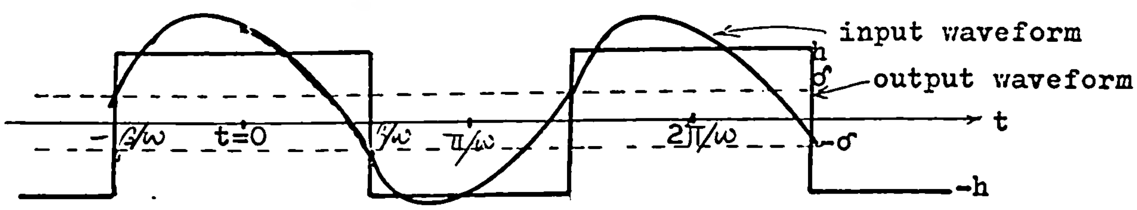

Fig.26 Input and output waveforms of on-off with hysteresis

Rewriting

$$\psi_1 = r_i - \sum_{n=1}^{\infty} a_n G_n \,(\cos n\beta \cos\varphi_n - \sin n\beta \sin\varphi_n) \qquad 106$$

$$\psi_2 = r_i - \sum_{n=1}^{\infty} a_n G_n \,(\cos n\beta \cos\varphi_n + \sin n\beta \sin\varphi_n) \qquad 107$$

Adding and subtracting the above give

$$\sum_{n=1}^{\infty} a_n G_n \cos n\beta \cos\varphi_n = r_i - \frac{\psi_1 + \psi_2}{2} \qquad 108$$

$$\sum_{n=1}^{\infty} a_n G_n \sin n\beta \sin\varphi_n = -\frac{\psi_2 - \psi_1}{2} \qquad 109$$

At the system oscillation frequency ω_o, we can write

$$G(jn\omega_o) = G_n \cos\varphi_n + jG_n \sin\varphi_n = \mathrm{Re}\left[G(jn\omega_o)\right] + j\,\mathrm{Im}\left[G(jn\omega_o)\right]$$

where Re and Im denote real part and imaginary part of the function respectively. Using this relationship and dividing eqns. 108 and 109 by $a_1 \cos\beta$ and $a_1 \sin\beta$ respectively

$$\frac{1}{a_1 \cos\beta} \sum_{n=1}^{\infty} a_n \cos n\beta \,\mathrm{Re}\left[G(jn\omega_o)\right] = \frac{2r_i - (\psi_1 + \psi_2)}{2a_1 \cos\beta} \qquad 110$$

$$\frac{1}{a_1 \sin\beta} \sum_{n=1}^{\infty} a_n \sin n\beta \,\mathrm{Im}\left[G(jn\omega_o)\right] = \frac{\psi_2 - \psi_1}{2a_1 \sin\beta} \qquad 111$$

For the on-off with hysteresis characteristic as shown in fig. 26, ψ_1 and ψ_2 are respectively

$$\psi_1 = +\delta \quad \text{and} \quad \psi_2 = -\delta \qquad 112$$

and

$$a_n = \frac{4h}{n\pi} \sin n\beta \,,$$ (from Appendix III)

Therefore

$$\sum_{n=1}^{\infty} \frac{1}{n} \frac{\sin n\beta}{\sin\beta} \frac{\cos n\beta}{\cos\beta} \, \mathrm{Re}\left[G(jn\omega_o)\right] = \frac{\pi \, r_i}{4h \, \sin\beta \, \cos\beta} \qquad 113$$

$$\sum_{n=1}^{\infty} \frac{1}{n} \left(\frac{\sin n\beta}{\sin\beta} \right)^2 \mathrm{Im}\left[G(jn\omega_o)\right] = \frac{-\delta\pi}{4h \, \sin^2\beta} \qquad 114$$

The describing function of this characteristic is found to be

$$D = \frac{4h}{\pi} \frac{\sin\beta}{\dfrac{r_i}{\cos\beta} - j\dfrac{\delta}{\sin\beta}} \qquad 115$$

And the critical response function which is defind to be $C = -\frac{1}{D}$

$$C = \frac{\pi r_i}{2h \, \sin 2\beta} - j\frac{\pi\delta}{4h \, \sin^2\beta} \qquad 116$$

The real and imaginary part of eqn.116 is seen to equal the right hand expression of eqns. 113 and 114 respectively.

Thus the left hand side of eqns. 113 and 114 indicate a sort of frequency response which varies according to the switching condition. If we draw the loci of the frequency response for several values of switching instant β and loci of the critical function which are also functions of switching instants, the oscillation frequency ω_o and β can be found.

2.4 Four Switching Conditions

Let us take the switching instants t as shown in fig. 27 and

$$t_1 = -\frac{\beta_1}{\omega}, \quad t_2 = -\frac{\beta_1}{\omega}, \quad t_3 = \frac{\pi - \beta_2}{\omega}, \quad \text{and } t_4 = \frac{\pi + \beta_2}{\omega} \text{※} \qquad 120$$

and the corresponsding instantaneous values for the input voltage e_i at the switching instants as ψ_1, ψ_2, ψ_3 and ψ_4.

Then we obtain following equations

$$\psi_1 = r_i - \sum_{n=1}^{\infty} a_n G_n \cos(-n\beta_1 - \varphi_n) \qquad 121$$

$$\psi_2 = r_i - \sum_{n=1}^{\infty} a_n G_n \cos(n\beta_1 - \varphi_n) \qquad 122$$

$$\psi_3 = r_i - \sum_{n=1}^{\infty} a_n G_n \cos(n\pi - n\beta_2 - \varphi_n) \qquad 123$$

$$\psi_4 = r_i - \sum_{n=1}^{\infty} a_n G_n \cos(n\pi + n\beta_2 - \varphi_n) \qquad 124$$

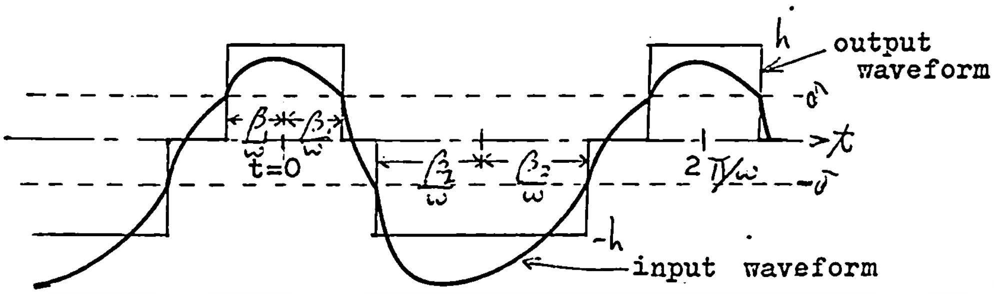

Fig. 27 Input and output waveforms of on-off with dead-zone

※ The assumption $t_{3,4} = \frac{\pi \pm \beta_2}{\omega}$ is only true when the system is symmetrical. For assymmetrical case, the value of $(\pi - d\beta)$ should be used instead of π in eqns.123 and 124. However, it makes the theory very complicated and there is no way to find exact value of $d\beta$.

Subtracting eqn. 121 from eqn. 123 gives

$$\psi_3-\psi_1 = -\sum_{n=1}^{\infty} a_n G_n(\cos n\pi\cos n\beta_2\cos\varphi_n-\cos n\pi\sin n\beta_2\sin\varphi_n -(\cos n\beta_1\cos\varphi_n-\sin n\beta_1\sin\varphi_n))$$

$$= -\sum_{n=1}^{\infty} a_n \operatorname{Re}\left[G(jn\omega)\right](\cos n\pi\cos n\beta_2-\cos n\beta_1) + \sum a_n \operatorname{Im}\left[G(jn\omega)\right](\cos n\pi\sin n\beta_2-\sin n\beta_1) \qquad 135$$

and eqn. 122 from 124

$$\psi_4-\psi_2 = -\sum_{n=1}^{\infty} a_n G_n(\cos n\pi\cos n\beta_2\cos\varphi_n+\cos n\pi\sin n\beta_2\sin\varphi_n -(\cos n\beta_1\cos\varphi_n+\sin n\beta_1\sin\varphi_n))$$

$$= -\sum_{n=1}^{\infty} a_n \operatorname{Re}\left[G(jn\omega)\right](\cos n\pi\cos n\beta_2-\cos n\beta_1) + \sum a_n \operatorname{Im}\left[G(jn\omega)\right](\cos n\pi\sin n\beta_2-\sin n\beta_1) \qquad 136$$

Adding eqn. 135 to 136 and subtracting 135 from 136 give respectively

$$-\frac{\psi_4+\psi_3-\psi_2-\psi_1}{2} = \sum_{n=1}^{\infty} a_n \operatorname{Re}\left[G(jn\omega)\right](\cos n\beta_1-\cos n\pi\cos n\beta_2) \qquad 137$$

$$-\frac{\psi_4+\psi_3+\psi_2-\psi_1}{2} = \sum_{n=1}^{\infty} a_n \operatorname{Im}\left[G(jn\omega)\right](\sin n\beta_1-\cos n\pi\sin n\beta_2) \qquad 138$$

Dividing the above two equations by $a_1(\cos\beta_1+\cos\beta_2)$ and $a_1(\sin\beta_1+\sin\beta_2)$ respectively gives

$$\sum_{n=1}^{\infty} \frac{a_n(\cos n\beta_1-\cos n\pi\cos n\beta_2)}{a_1(\cos\beta_1+\cos\beta_2)} \operatorname{Re}\left[G(jn\omega)\right] = \frac{\psi_1+\psi_2-\psi_3-\psi_4}{2a_1(\cos\beta_1+\cos\beta_2)} \qquad 139$$

for $0\leq\beta_1,\ \beta_2\leq\pi$ and $\beta_1\neq\pi-\beta_2$

$$\sum_{n=1}^{\infty} \frac{a_n(\sin n\beta_1-\cos n\pi\sin n\beta_2)}{a_1(\sin\beta_1+\sin\beta_2)} \operatorname{Im}\left[G(jn\omega)\right] = \frac{\psi_1-\psi_2-\psi_3+\psi_4}{2a_1(\sin\beta_1+\sin\beta_2)} \qquad 140$$

for $0\leq\beta_1,\ \beta_2\leq\pi$ and $\beta_1\neq\beta_2$

Let $\text{Re}\left[A(j\omega)\right]_\beta$ and $\text{Im}\left[A(j\omega)\right]_\beta$ denote the lefthand side expressions of eqns. 139 and 140 respectively. Again if the appropriate values of ψ's for a particular non-linear characteristic are used, it is found that the right-hand expressions of eqns. 139 and 140 become the real and imaginary parts of the critical function C. Therefore the relationship between $\left[A(j\omega)\right]_\beta$ and $C(\beta)$ is simply

$$\left[A(j\omega)\right]_\beta = C(\beta) \qquad 141$$

where $\left[A(j\omega)\right]_\beta$ can be called the modified frequency response.

Furthermore, adding eqns. 121, 122, 123 and 124 gives

$$r_i = \frac{\psi_1+\psi_2+\psi_3+\psi_4}{4} + \frac{1}{2}\sum_{n=1}^{\infty} a_n(\cos n\beta_1+\cos n\pi\cos n\beta_2)\text{Re}\left[G(jn\omega)\right] \qquad 142$$

This equation gives additional information regarding the d.c. input. After evaluating the oscillating frequency from eqn. 140, the required d.c. input to the non-linearity can be found by substituting this frequency to eqn. 142. The required d.c. input to the system is the sum of the above value and the d.c. component of the feedback signal.

For the particular cases of $\beta_1+\beta_2=\pi$, or $\beta_1=\beta_2$ equations 139 and 140 should be modified to avoid that the denominators become zero. These cases reduce to two-switching condition.

(a) When $\beta_1+\beta_2=\pi$ 143

Let $\beta_1=\beta$, $\beta_2=\pi-\beta-\gamma$

where γ is a small angle. Now, the real part is, from eqn. 139

$$\mathrm{Re}\left[A(j\omega)\right]_{\beta_1\beta_2} = \sum_{n=1}^{\infty} \frac{a_n(\cos n\beta-(\cos n\pi)^2(\cos n\beta\cos n\gamma-\sin n\beta\sin n\gamma))}{a_1(\cos\beta+\cos\pi(\cos\beta\cos\gamma-\sin\beta\sin\gamma))}\mathrm{Re}\left[G(jn\omega)\right]$$

$$= \sum_{n=1}^{\infty} \frac{a_n(\cos n\beta(1-\cos n\gamma)+\sin n\beta\sin n\gamma)}{a_1(\cos\beta(1-\cos\gamma)+\sin\beta\sin\gamma)}\mathrm{Re}\left[G(jn\omega)\right].$$

Taking the limit for $\gamma\to 0$

$$\mathrm{Re}\left[A(j\omega)\right]_{\beta} = \lim_{\gamma\to 0}\mathrm{Re}\left[A(j\omega)\right]_{\beta_1,\beta_2}$$

$$= \sum_{n=1}^{\infty}\lim_{\gamma\to 0}\frac{a_n}{a_1}\,\frac{\dfrac{\cos n\beta(1-\cos n\gamma)}{\sin\beta\sin\gamma}+\dfrac{\sin n\beta\sin n\gamma}{\sin\beta\sin\gamma}}{\dfrac{\cos\beta(1-\cos\gamma)}{\sin\beta\sin\gamma}+1}\mathrm{Re}\left[G(jn\omega)\right]$$

$$= \sum_{n=1}^{\infty}\frac{a_n}{a_1}\,n\,\frac{\sin n\beta}{\sin\beta}\mathrm{Re}\left[G(jn\omega)\right] \qquad 144$$

And for the imaginary part, letting $\beta_1=\beta$, $\beta_2=\pi-\beta$

$$\mathrm{Im}\left[A(j\omega)\right]_{\beta} = \sum_{n=1}^{\infty}\frac{a_n}{a_1}\,\frac{\sin n\beta+(\cos n\pi)^2\sin n\beta}{\sin\beta-\cos n\pi\sin\beta}\,\mathrm{Im}\left[G(jn\omega)\right]$$

$$= \sum_{n=1}^{\infty}\frac{a_n}{a_1}\,\frac{\sin n\beta}{\sin\beta}\,\mathrm{Im}\left[G(jn\omega)\right] \qquad 145$$

(b) When $\beta_1=\beta_2=\beta$, but $0<\beta<\pi/2$ 146

$$\mathrm{Re}\left[A(jn\omega)\right]_{\beta} = \sum_{n=1}^{\infty}\frac{a_n}{a_1}\,\frac{(1-\cos n\pi)\cos n\beta}{2\cos\beta}\,\mathrm{Re}\left[G(jn\omega)\right]$$

$$= \sum_{n=1}^{\infty}\frac{a_n}{a_1}\,\frac{\sin^2(n\pi/2)\cos n\beta}{\cos\beta}\,\mathrm{Re}\left[G(jn\omega)\right]. \qquad 147$$

$$\mathrm{Im}\left[A(jn\omega)\right]_{\beta} = \sum_{n=1}^{\infty}\frac{a_n}{a_1}\,\frac{\sin^2(n\pi/2)\sin n\beta}{\sin\beta}\,\mathrm{Im}\left[G(jn\omega)\right] \qquad 148$$

(c) When $\beta_1 = \beta_2 = \pi/2$ 149

From the result in case (a), we get the finite value of $\mathrm{Re}\left[A(jn\omega)\right]$

$$\mathrm{Re}\left[A(jn\omega)\right]_{\pi/2} = \sum_{n=1}^{\infty} \frac{a_n}{a_1} \sin(n\pi/2)\ n\ \mathrm{Re}\left[G(jn\omega)\right] \qquad 150$$

The same result can be derived from case (b).

3 Application to Particular Systems

3.1 General Procedure

The general method to obtain a solution is to (a) plot the modified frequency response function $\left[A(j\lambda)\right]_{\beta}$ (where $\lambda = \omega T$) as a function of λ for various values of the angle β on the complex plane together with the critical function with the corresponding β, (b) determine any intersection of the loci with the same value of β thus evaluate the oscillating frequency λ. Analytical expressions for the summation of the infinite series can be found, however, to obtain solution most of the computaion was done on the IBM 7040 computer.

Four examples were attempted to apply the theory to actual systems with the linear transfer functions $\frac{K}{1+sT}$ and $\frac{K}{(1+sT)^2}$. in combination with the three kinds of non-linear characteristics in the manner listed below .

(1) On-off with hysteresis and $G(s) = \frac{K}{1+sT}$.

(2) On-off with hysteresis and $G(s) = \frac{K(1-sT)}{(1+sT)^2}$

(3) On-off with dead-zone and $G(s) = \frac{K(1-sT)}{(1+sT)^2}$

(4) Saturation (symmetrical case) and $G(s) = \frac{K(1-sT)}{(1+sT)^2}$

3.2 On-Off with Hysteresis and $G(s) = \frac{K}{1 + sT}$

Substituting $s = j\omega$, the linear transfer function becomes

$$G(j\omega) = \frac{K}{1+\omega^2T^2} - j\frac{K\omega T}{1+\omega^2T^2} \qquad 152$$

Thereby, using equs. 113 and 114, and substituting $\lambda=\omega T$

$$\sum_{n=1}^{\infty}\frac{1}{n}\,\frac{\sin n\beta}{\sin\beta}\,\frac{\cos n\beta}{\cos\beta}\,\frac{K}{1+n^2\lambda^2} = \frac{r_i\pi}{4h\,\sin\beta\cos\beta} \qquad 153$$

$$\sum_{n=1}^{\infty}\frac{1}{n}\left(\frac{\sin n\beta}{\sin\beta}\right)^2\frac{-Kn\lambda}{1+n^2\lambda^2} = \frac{-\delta\pi}{4h\,\sin^2\beta} \qquad 154$$

As already stated the left-hand side of the above equations are respectively the real and imaginary part of the modified frequency response $\left[A(jn\lambda)\right]_{\beta}$ and the right-hand side the critical function of the on-off with hysteresis characteristic.

For the above simple case a graphical solution is not necessary since, we may write

$$\frac{r_i}{hK} = \frac{2}{\pi}\sum_{n=1}^{\infty}\frac{\sin 2n\beta}{n(1+n^2\lambda^2)} \qquad 155$$

$$\frac{\delta}{hK} = \frac{2\lambda}{\pi}\sum_{n=1}^{\infty}\frac{1-\cos 2n\beta}{(1+n^2\lambda^2)} \qquad 156$$

The infinite summations in the above equations have the analytical solutions. By the help of Appendix II, we have

$$\sum_{n=1}^{\infty}\frac{\sin 2n\beta}{n(1+n^2\lambda^2)} = \frac{\pi}{2}\left(1 - \frac{\sinh((\pi-2\beta)/\lambda)}{\sinh(\pi/\lambda)}\right) - \beta \qquad 157$$

and

$$\sum_{n=1}^{\infty}\frac{\cos 2n\beta}{1+n^2\lambda^2} = \frac{\pi}{2}\left(\frac{\cosh((\pi-2\beta)/\lambda)}{\sinh(\pi/\lambda)}\right) - \frac{1}{2} \qquad 158$$

Hence,

$$\frac{r_i}{hK} = \left(1 - \frac{\sinh((\pi-2\beta)/\lambda)}{\sinh(\pi/\lambda)}\right) - \frac{2\beta}{\pi} \qquad 159$$

$$\frac{\delta}{hK} = \frac{\cosh(\pi/\lambda) - \cosh((\pi-2\beta)/\lambda)}{\sinh(\pi/\lambda)} \qquad 160$$

The d.c. component of input to non-linearity is the difference of d.c. input to the system and the d.c. component of the system output. The output d.c. component is $h(\frac{2}{\beta}-1)$ and G(s) has gain K at zero frequency. Therefore the required system input is from

$$r_i = r - Kh(\frac{2\beta}{\pi}-1),$$

$$\frac{r}{hK} = \frac{\sinh((\pi-2\beta)/\lambda)}{\sinh(\pi/\lambda)} \qquad 161$$

Graphs in fig. 28 show the relationship between $\frac{\delta}{hK}$ and $\frac{r}{hK}$ taking λ as a parameter. Eliminating β graphically from fig.28, a relationship between the normalized oscillating frequency, λ, and normalized hysteresis, δ/hK, taking normalized d.c. input, r/hK, as a parameter, is found and shown in fig. 29.

These theoretical results are compared with the results from the analog computer simulation in fig. 30. The experiments were made in three cases;

(a) constant d.c. input, and variable gain K

(b) constant gain K and variable d.c. input r

(c) no d.c. input and variable gain K

The points marked by x on the graph are measured ones, and the continuous lines represent the theoretically predicted values for λ.

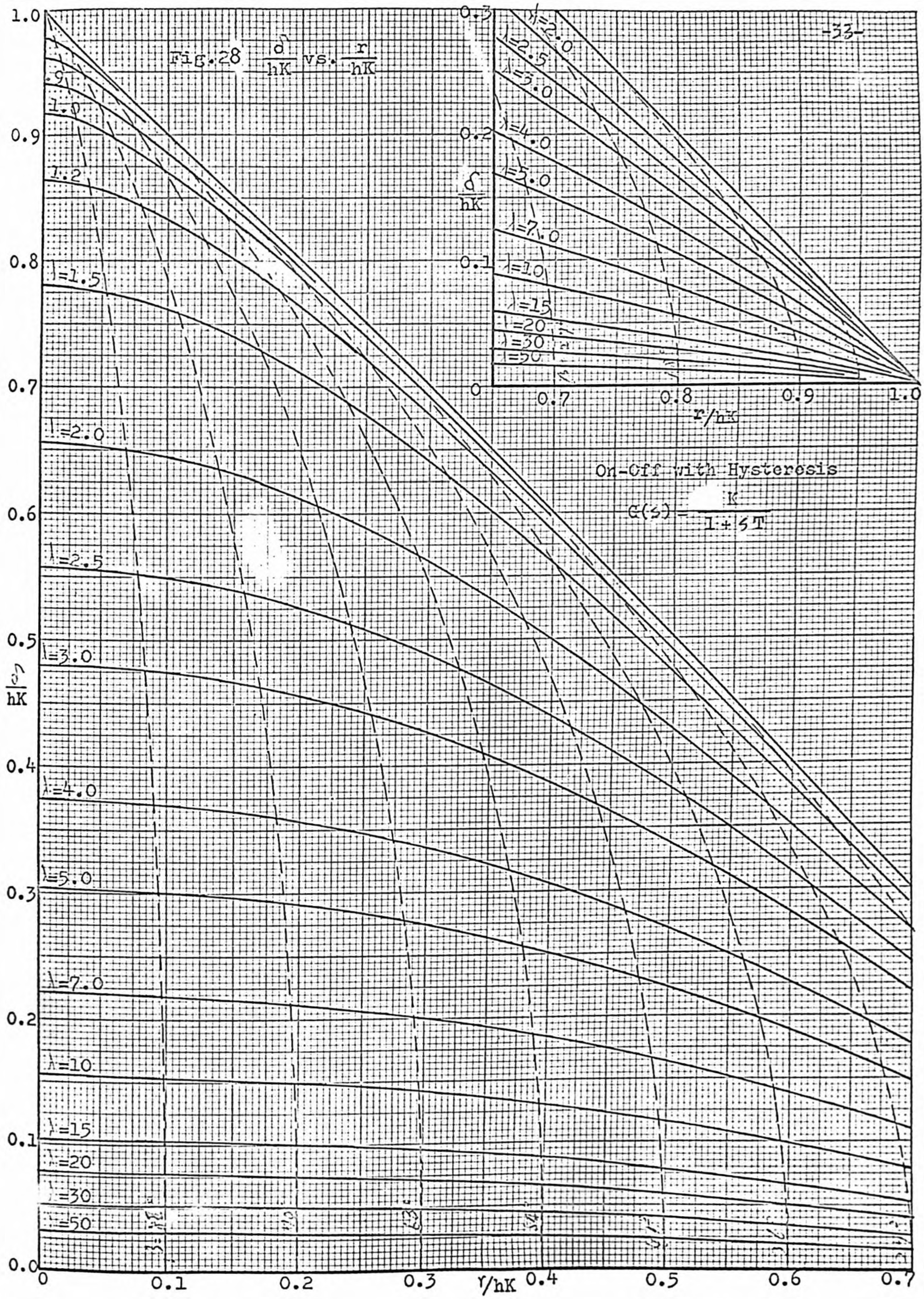

Fig.28 $\frac{\delta}{hK}$ vs. $\frac{r}{hK}$
On-Off with Hysteresis
$G(s) = \frac{K}{1+sT}$
$\frac{\delta}{hK}$
r/hK
λ=1.5
λ=2.0
λ=2.5
λ=3.0
λ=4.0
λ=5.0
λ=7.0
λ=10
λ=15
λ=20
λ=30
λ=50
1.0
1.2
0.0
0.1
0.2
0.3
0.4
0.5
0.6
0.7
0.8
0.9
1.0

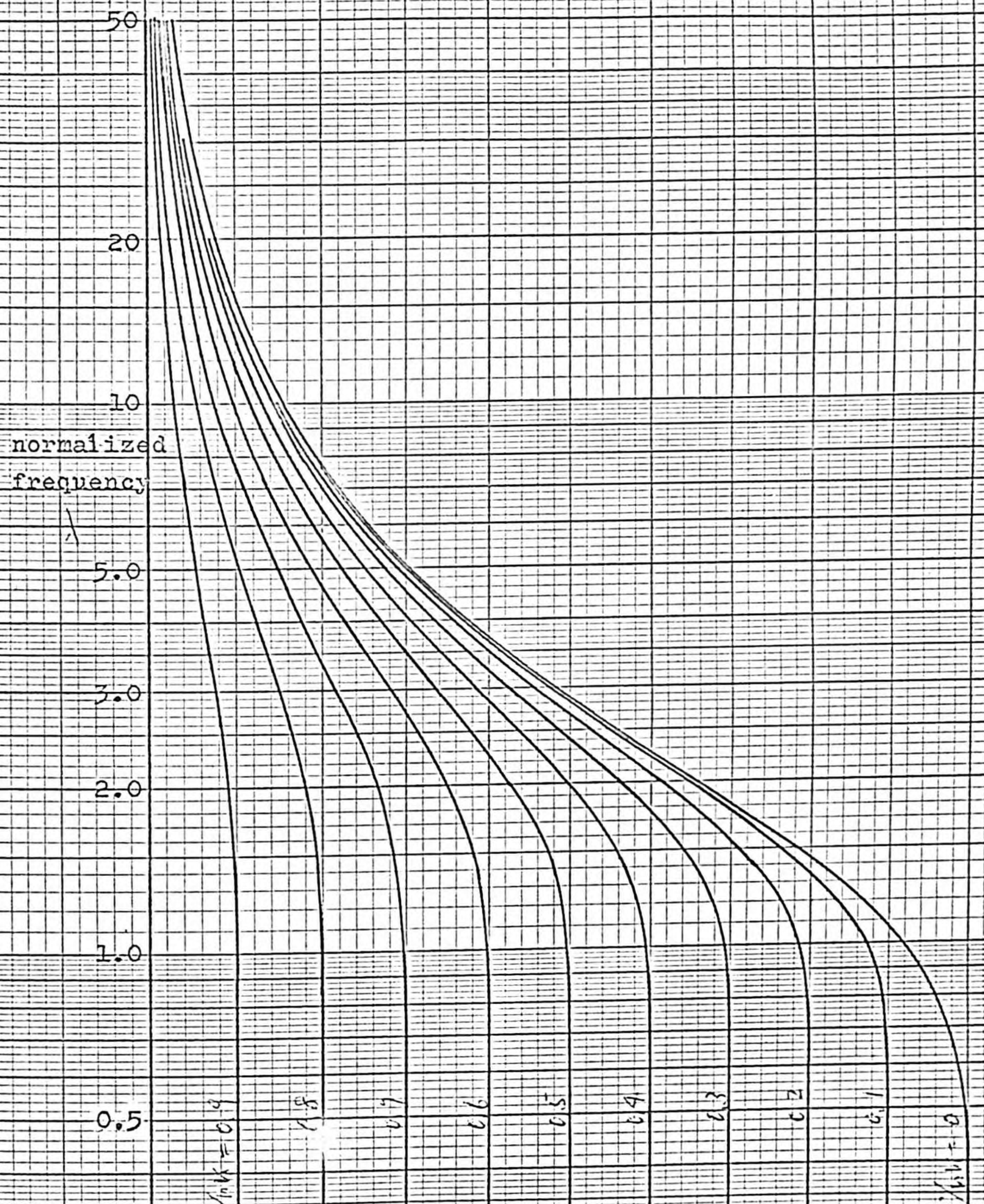

Fig.29 Oscillating Frequency, on-off with hysteresis and $G(s) = \frac{K}{1 + sT}$

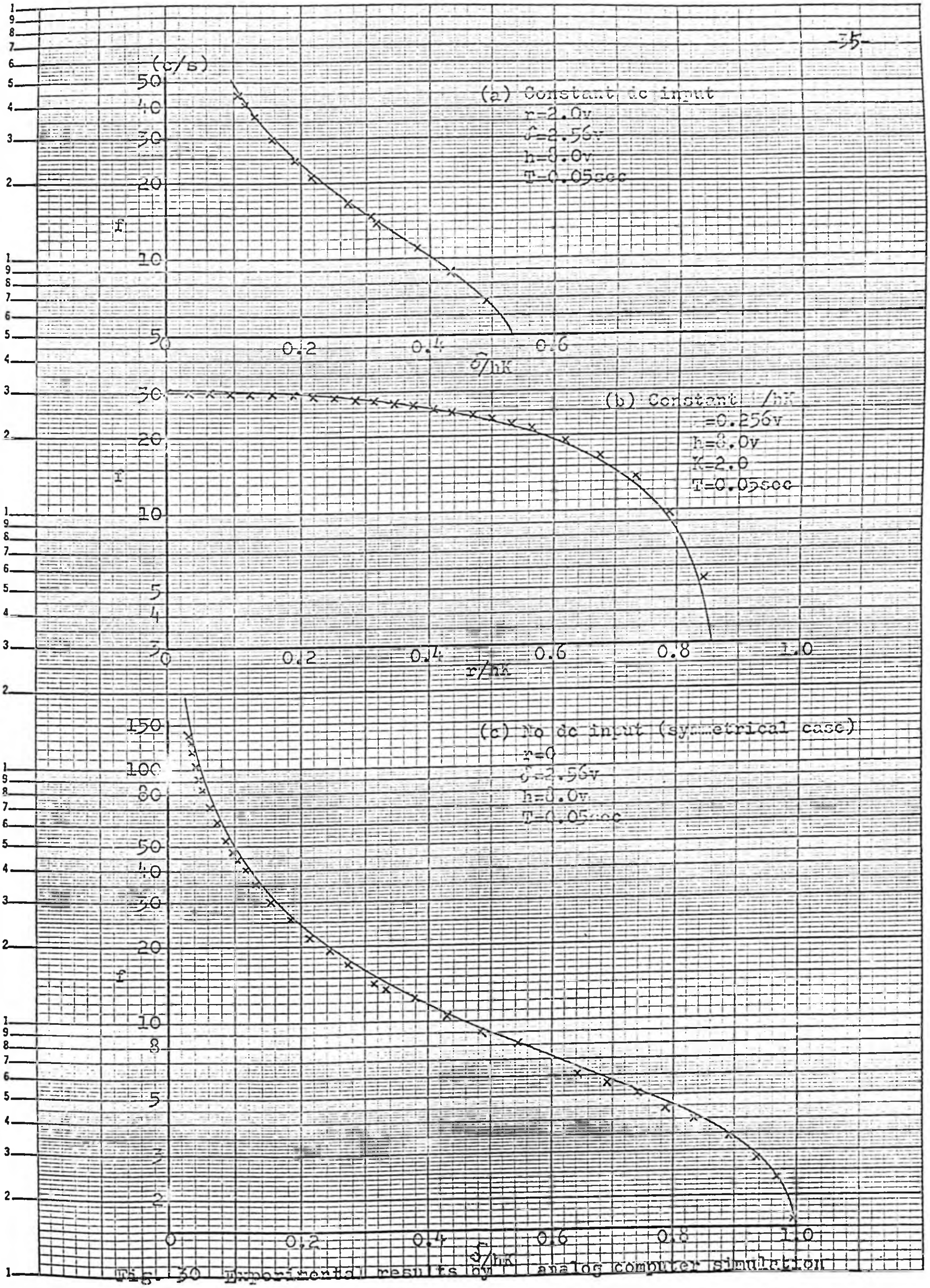

Fig. 30 Experimental results by analog computer simulation

3.3 On-Off with Hysteresis and $G(s) = \frac{K(1 - sT)}{(1 + sT)^2}$

This is same as the previous example except that the linear transfer function is changed to $G(s) = \frac{K(1-sT)}{(1+sT)^2}$. In this example, we transfer the linear gain K from the linear part to the non-linear part. It does not lose the generality, and eliminates the necessity of drawing the frequency response loci with various value of K. The output of the on-off with hysteresis now can be considered as Kh instead of h. The real and imaginary parts of the transfer function become

$$\mathrm{Re}\left[G(jn\lambda)\right] = \frac{1 - 3n^2\lambda^2}{(1 + n^2\lambda^2)^2} \tag{163}$$

$$\mathrm{Im}\left[G(jn\lambda)\right] = \frac{-n\lambda(3 - n^2\lambda^2)}{(1 + n^2\lambda^2)^2} \tag{164}$$

where $\lambda = \omega T$. Therefore the modified frequency response locus is expressed by the equations

$$\mathrm{Re}\left[A(j\lambda)\right]_\beta = \frac{1}{\sin 2\beta} \sum_{n=1}^{\infty} \frac{\sin 2n\beta\,(1-3n^2\lambda^2)}{n(1+n^2\lambda^2)^2} \tag{165}$$

and

$$\mathrm{Im}\left[A(j\lambda)\right]_\beta = -\frac{1}{\sin^2\beta} \sum_{n=1}^{\infty} \frac{\sin^2 n\beta \cdot \lambda(3-n^2\lambda^2)}{(1+n^2\lambda^2)^2} \tag{166}$$

While the critical function is

$$C(\beta) = \frac{r_i\pi}{2hK\sin 2\beta} - j\frac{\delta\pi}{4hK\sin^2\beta} \tag{167}$$

Rewriting equs. 165 and 166

$$\mathrm{Re}\left[A(j\lambda)\right]_\beta = \frac{1}{\sin 2\beta}\left\{\sum_{n=1}^{\infty}\frac{\sin 2n\beta}{n(1+n^2\lambda^2)} - 4\lambda^2\sum_{n=1}^{\infty}\frac{n\sin 2n\beta}{(1+n^2\lambda^2)^2}\right\} \tag{168}$$

and

$$\text{Im}\left[A(j\lambda)\right] = -\frac{\lambda}{2\sin^2\beta}\left\{\sum_{n=1}^{\infty}\frac{3}{(1+n^2\lambda^2)^2} - \sum_{n=1}^{\infty}\frac{n^2\lambda^2}{(1+n^2\lambda^2)^2} - \sum_{n=1}^{\infty}\frac{3\cos 2n\beta}{(1+n^2\lambda^2)^2} + \sum_{n=1}^{\infty}\frac{n^2\lambda^2\cos 2n\beta}{(1+n^2\lambda^2)^2}\right\} \quad 169$$

From the definition of Appendix II, we can write

$$\text{Re}\left[A(j\lambda)\right]_\beta = \frac{1}{\sin 2\beta}\left\{S_{-1,1}(\lambda,2\beta) - 4\lambda^2\, S_{1,2}(\lambda,2\beta)\right\} \quad 170$$

$$\text{Im}\left[A(j\lambda)\right]_\beta = -\frac{1}{2\sin^2\beta}\left\{3\left[C_{0,1}(\lambda,0) - C_{0,1}(\lambda,2\beta)\right] - 4\lambda^2\left[C_{2,2}(\lambda,0) - C_{2,2}(\lambda,2\beta)\right]\right\} \quad 171$$

where

$$S_{-1,1}(\lambda,2\beta) = \sum_{n=1}^{\infty}\frac{n^{-1}\sin 2n\beta}{(1+n^2\lambda^2)} \quad 172$$

$$S_{1,2}(\lambda,2\beta) = \sum_{n=1}^{\infty}\frac{n\ \sin 2n\beta}{(1+n^2\lambda^2)^2} \quad 173$$

$$C_{0,1}(\lambda,2\beta) = \sum_{n=1}^{\infty}\frac{\cos 2n\beta}{(1+n^2\lambda^2)} \quad 174$$

$$C_{2,2}(\lambda,2\beta) = \sum_{n=1}^{\infty}\frac{n^2\ \cos 2n\beta}{(1+n^2\lambda^2)^2} \quad 175$$

The values of $A(j\lambda)$ with several angles of β were calculated by means of the computer. Fig. 31 shows the required modified frequency response loci.

From the modified frequency response loci and the describing function the relationship between the hysteresis width δ, the output of non-linear characteristic, h, linear gain K, and oscillation frequency is given by

$$\frac{\delta}{hK} = \frac{4}{\pi} \sin^2\beta \ \mathrm{Im}\left[A(j\lambda)\right]_\beta \qquad 176$$

and the d.c. input to the system r is

$$\frac{r}{hK} = \frac{2}{\pi} \sin 2\beta \ \mathrm{Re}\left[A(j\lambda)\right]_\beta + \frac{2}{\pi}\beta - 1 \qquad 177$$

By eliminating β from eqns. 176 and 177, an explicit relationship between δ/hK, r/hK and λ is obtained. Fig. 32 shows the relation λ versus δ/hK with r/hK as a parameter, and fig. 33 r/hK and δ/hK with λ or β as a parameter. Using either of the graphs, the oscillation frequency of the system can be predicted theoretically knowing the hysteresis constants δ and h, the system d.c. input r, linear gain K, and time constant T.

Again the results are compared with the experimental results in fig. 34.

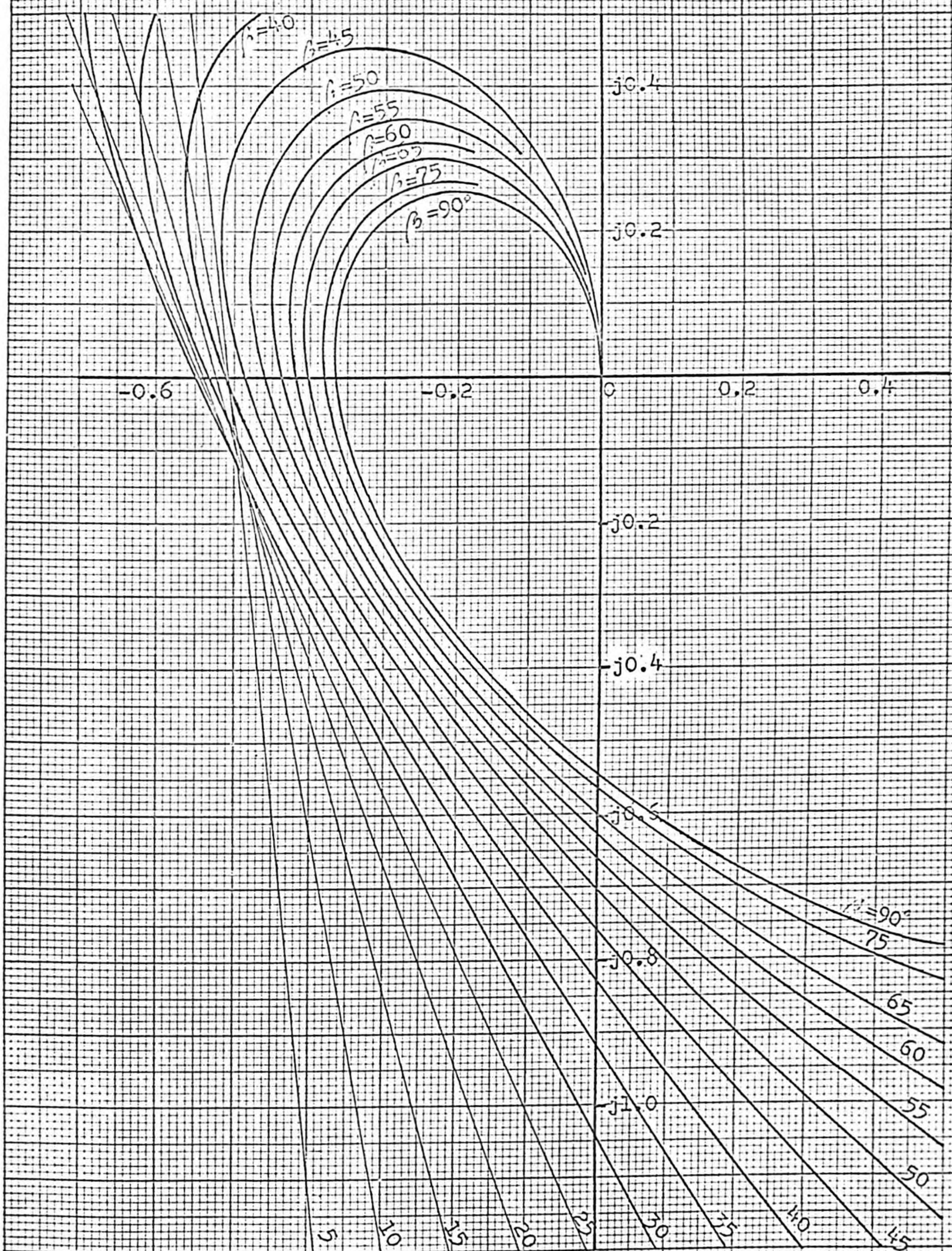

Fig. 31 Modified frequency response loci

On-off with hysteresis and $G(s) = \frac{1-sT}{(1+sT)^2}$

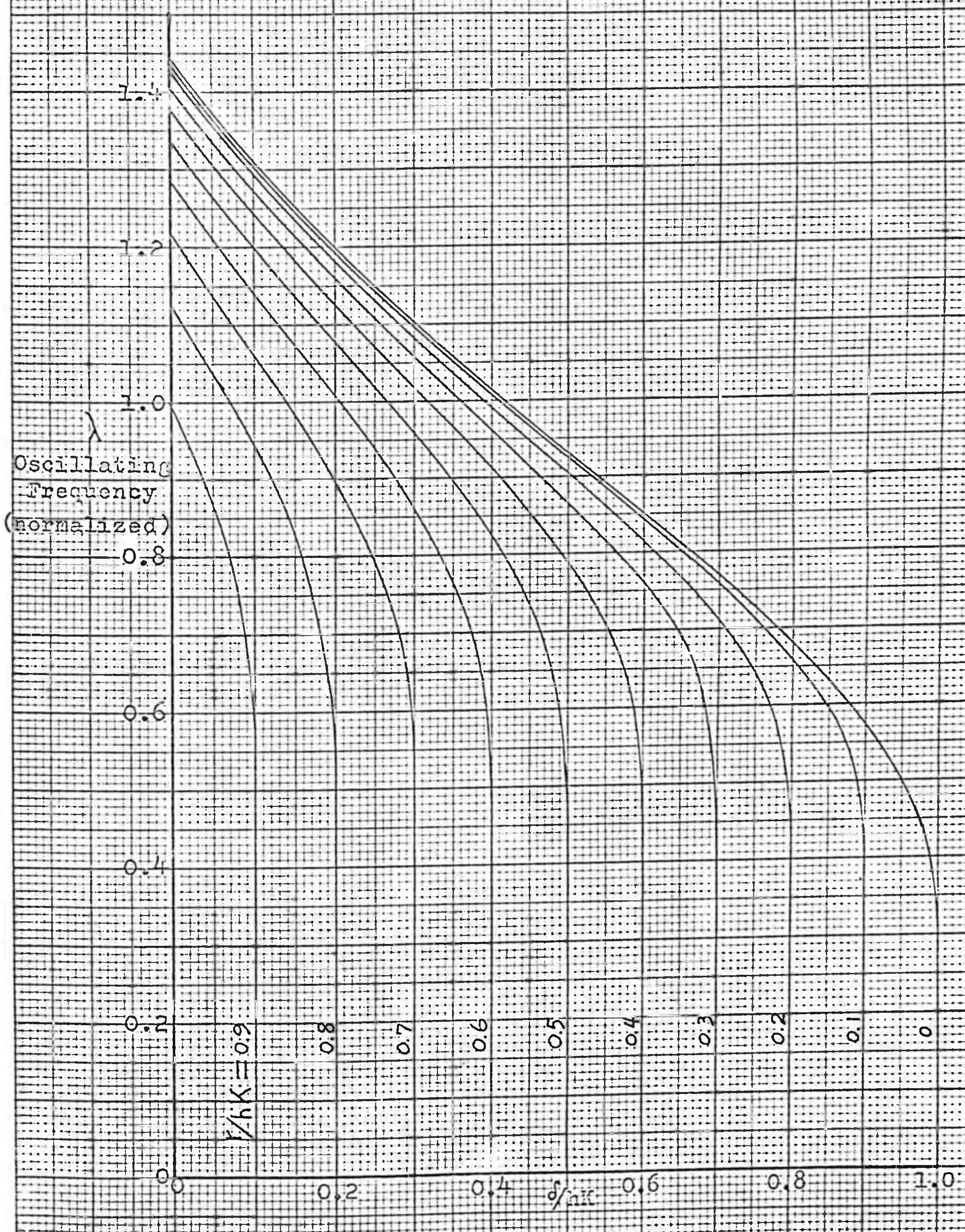

Fig. 32 Oscillating frequency vs. non-linearity constants

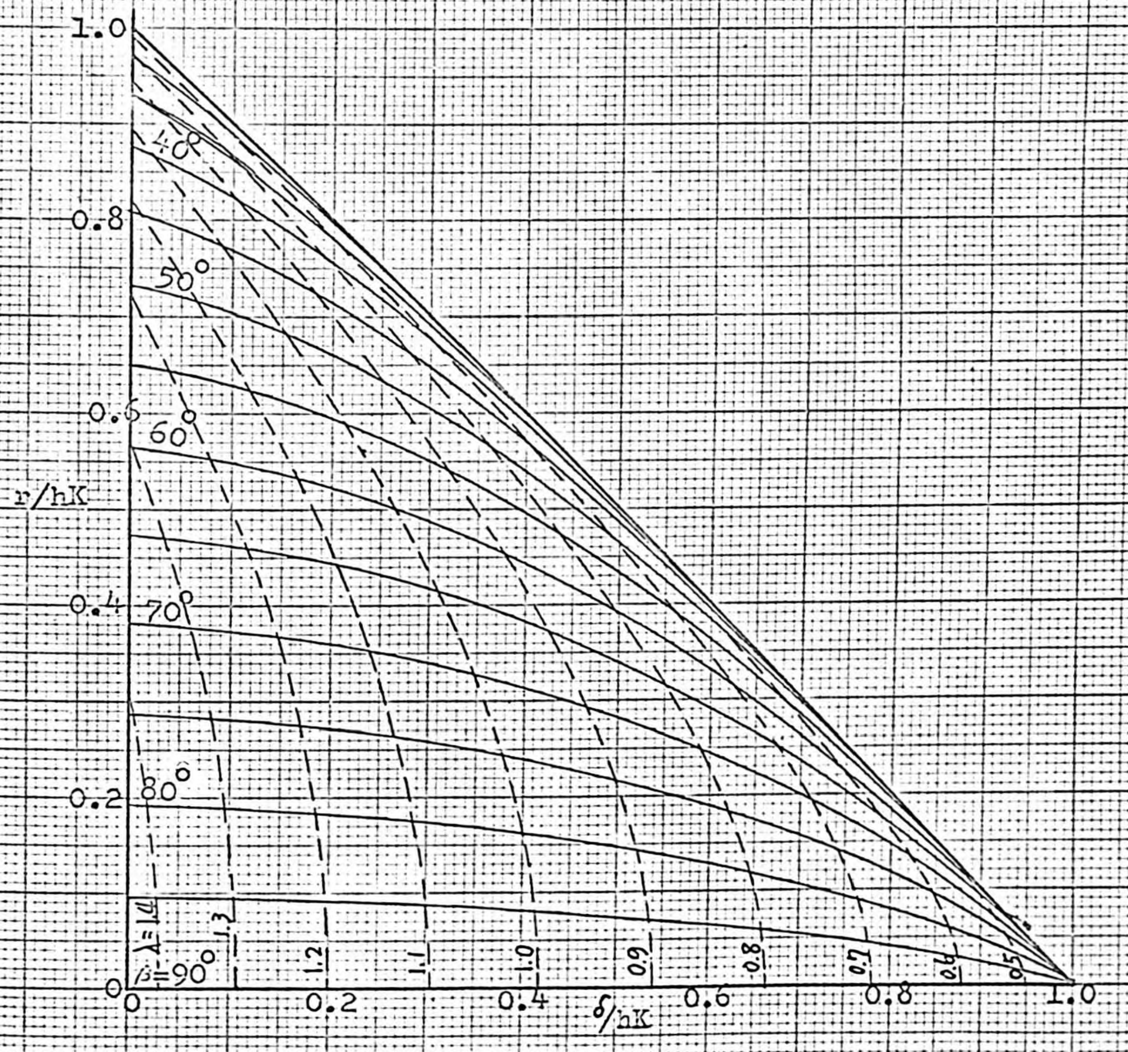

Fig. 33 Non-linearity constants and dc input vs. oscillating frequency and switching angle

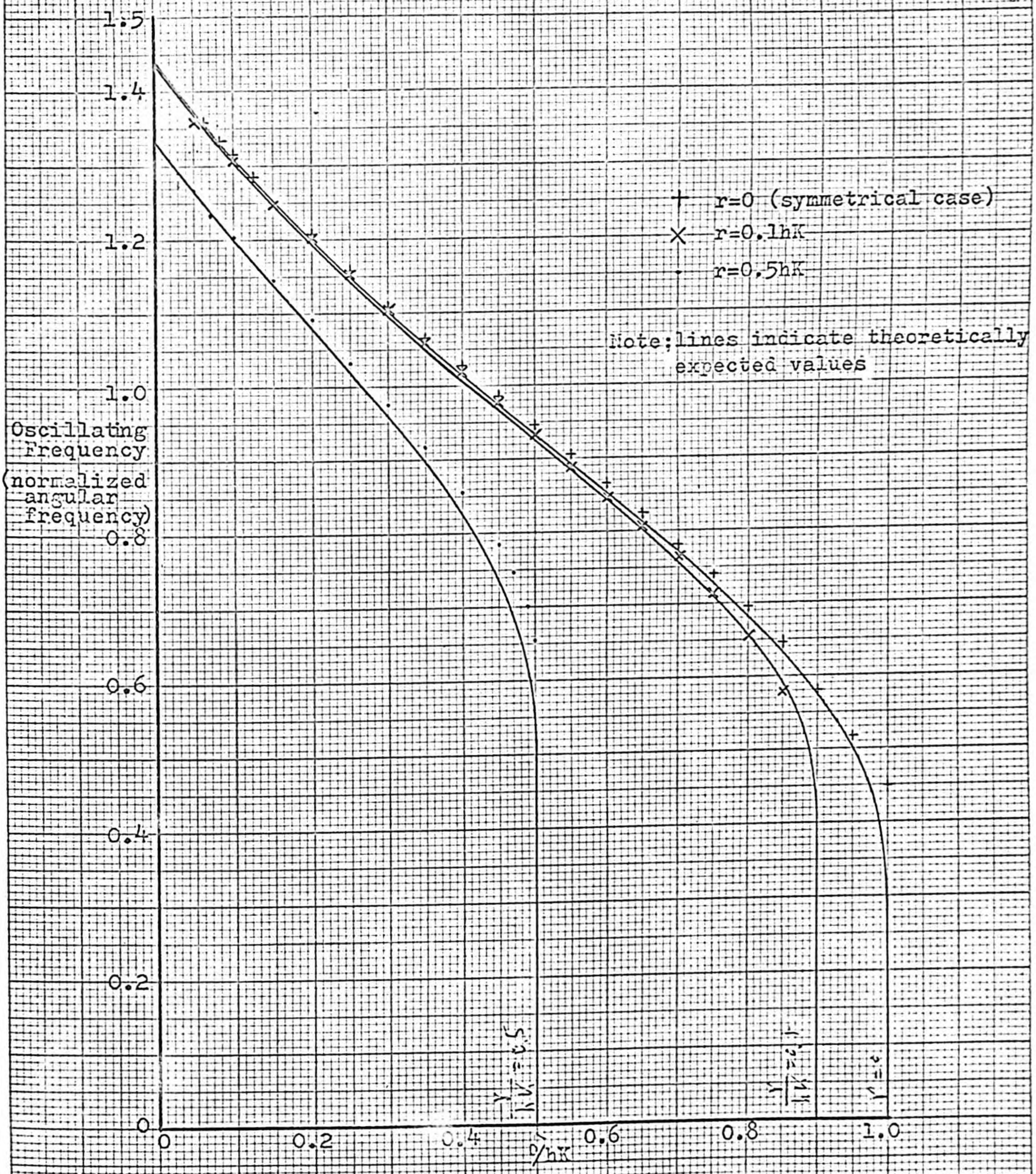

Fig. 34 Experimental result by simulation

3.4 On-Off with Dead-Zone and $G(s) = \dfrac{K(1-sT)}{(1+sT)^2}$

Again the basic configuration shown in fig. 24 is considered where the linear network G(s) is the same as the previous example and the non-linear characteristic is shown in fig. 25 (c). Operation of the system with the existence of d.c. input is shown in fig. 27. This is an example of four switching conditions. Substituting the given values for G(s) and the non-linear characteristic in the left-hand side expressions of eqns. 139 and 140, and in eqn. 142 the following results for the infinite summations, are obtained:

$$\mathrm{Re}^*\left[A(j\lambda)\right]_{\beta_1\beta_2} = \tfrac{1}{2}S_{-1,1}(\lambda,2\beta_1)+\tfrac{1}{2}S_{-1,1}(\lambda,2\beta_2)+S_{-1,1}(\lambda,\pi-\beta_1-\beta_2)$$
$$-4\lambda^2\left\{\tfrac{1}{2}S_{1,2}(\lambda,2\beta_1)+\tfrac{1}{2}S_{1,2}(\lambda,2\beta_2)+S_{1,2}(\lambda,\pi-\beta_1+\beta_2)\right\} \qquad 178$$

$$\mathrm{Im}^*\left[A(j\lambda)\right]_{\beta_1\beta_2} = 4\lambda^3\Big\{C_{2,2}(\lambda,0)-\tfrac{1}{2}C_{2,2}(\lambda,2\beta_1)-\tfrac{1}{2}C_{2,2}(\lambda,2\beta_2)-C_{2,2}(\lambda,\pi-\beta_1+\beta_2)$$
$$+C_{2,2}(\lambda,\pi-\beta_1-\beta_2)\Big\} - 3\lambda\Big\{C_{0,1}(\lambda,0)-\tfrac{1}{2}C_{0,1}(\lambda,2\beta_1)-\tfrac{1}{2}C_{0,1}(\lambda,2\beta_2)$$
$$-C_{0,1}(\lambda,\pi-\beta_1+\beta_2)+C_{0,1}(\lambda,\pi-\beta_1-\beta_2)\Big\} \qquad 179$$

where

$$\mathrm{Re}^*\left[A(j\lambda)\right]_{\beta_1\beta_2} = \frac{1}{K}(\cos\beta_1+\cos\beta_2)(\sin\beta_1+\sin\beta_2)\mathrm{Re}\left[A(j\lambda)\right]_{\beta_1\beta_2} \qquad 180$$

$$\mathrm{Im}^*\left[A(j\lambda)\right]_{\beta_1\beta_2} = \frac{1}{K}(\sin\beta_1+\sin\beta_2)^2\mathrm{Im}\left[A(j\lambda)\right]_{\beta_1\beta_2} \qquad 181$$

and

$$\frac{r_i}{hK} = \frac{1}{2\pi}\left\{S_{-1,1}(\lambda,2\beta_1)-S_{-1,1}(\lambda,2\beta_2)-2S_{-1,1}(\lambda,\pi-\beta_1+\beta_2)\right.$$
$$\left.-4\lambda^2\left[S_{1,2}(\lambda,2\beta_1)-S_{1,2}(\lambda,2\beta_2)-2S_{1,2}(\lambda,\pi-\beta_1+\beta_2)\right]\right\} \qquad 182$$

Again, we also have the d.c. relationship

$$\frac{r}{hK} = \frac{r_i}{hK} - \frac{\beta_1 - \beta_2}{\pi} \qquad 183$$

To include the case where the dead-zone is zero, using eqns. 144 and 145, when $\beta_2 = \pi - \beta_1 = \beta$

$$\mathrm{Re}\left[A(j\lambda)\right]_\beta = \frac{1}{2\sin^2\beta}\left\{C_{0,1}(\lambda,0)-C_{0,1}(\lambda,2\beta)\right.$$
$$\left.-4\lambda^2\left[C_{2,2}(\lambda,0)-C_{2,2}(\lambda,2\beta)\right]\right\} \qquad 184$$

and

$$\mathrm{Im}\left[A(j\lambda)\right]_\beta = \frac{-\lambda}{2\sin^2\beta}\left\{3\left[C_{0,1}(\lambda,0)-C_{0,1}(\lambda,2\beta)\right]\right.$$
$$\left.-4\lambda^2\left[C_{2,2}(\lambda,0)-C_{2,2}(\lambda,2\beta)\right]\right\} \qquad 185$$

Thus plotting the loci $\left[A\,(j\lambda)\right]_{\beta_1\beta_2}$ and the critical function for the non-linearity as a function of βs for the same value of βs, the normalized frequency of oscillation, λ, can be found and then using eqns. 182 and 183 the required reference value, r.

The loci with K=1 for several values of β_1 and β_2 are shown in fig. 35, 36, and 37. The results of the numerical calculation for the relationship between δ/hK, r/hK and λ are shown in fig. 38 and 39.

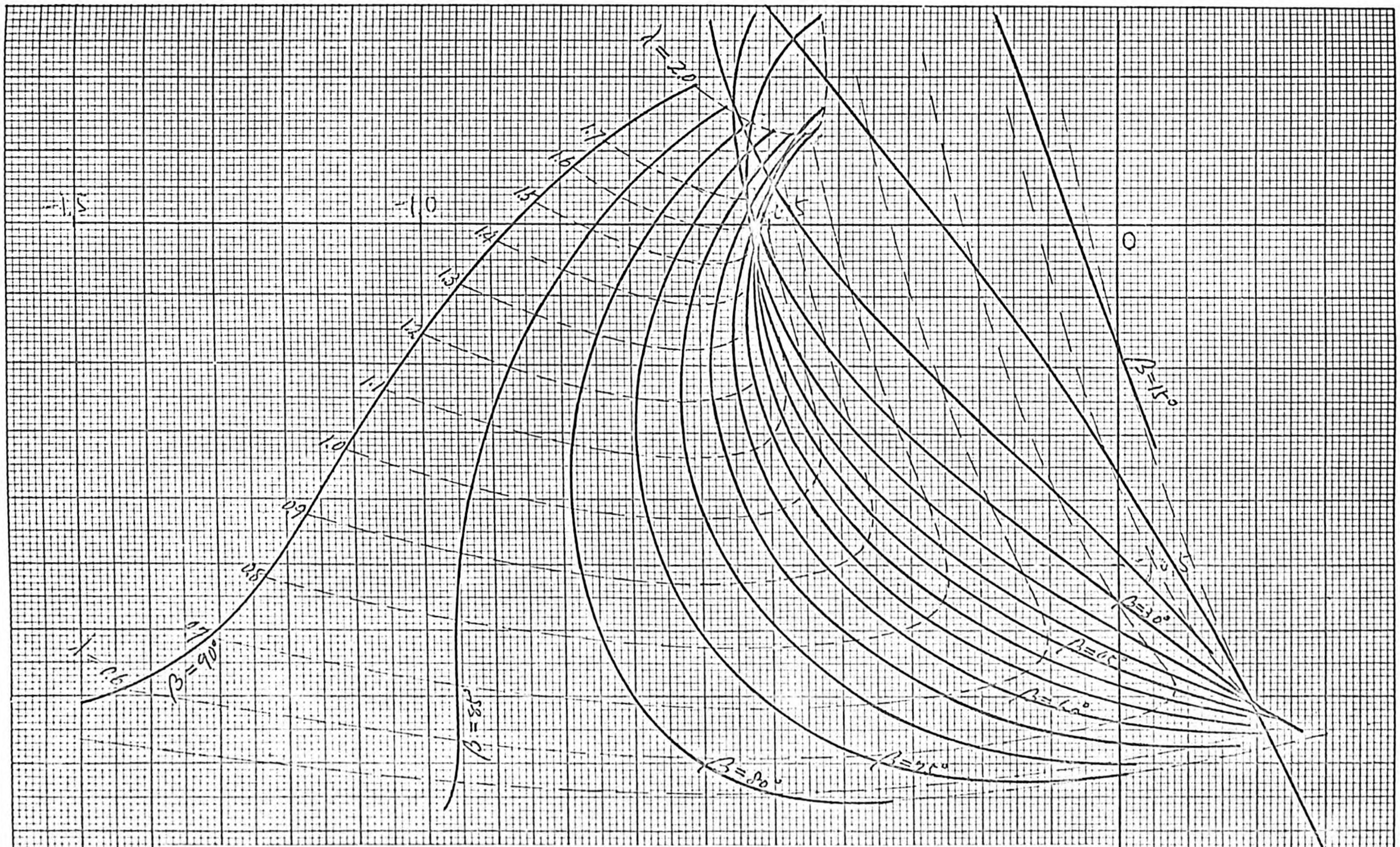

Fig. 35 Modified frequency response loci for on-off with dead-zone and $G(s)=\dfrac{1-sT}{(1+sT)^2}$, symmetrical case ($\beta_1=\beta_2=\beta$)

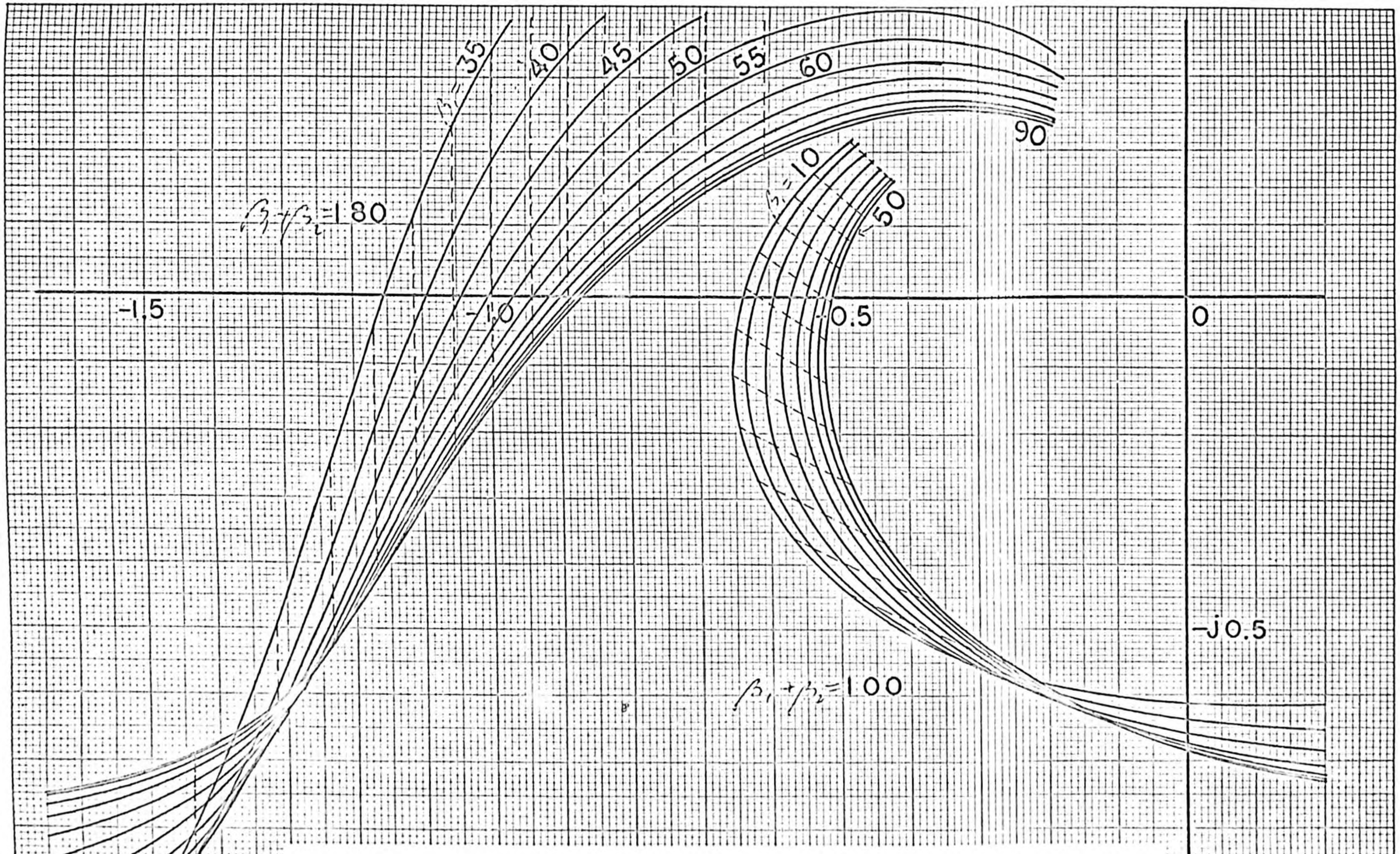

Fig. 36 Modified frequency response loci for on-off with dead-zone and $G(s) = \dfrac{1-sT}{(1+sT)^2}$, when $\beta_1+\beta_2 = 100^\circ$ and $\beta_1+\beta_2 = 180^\circ$

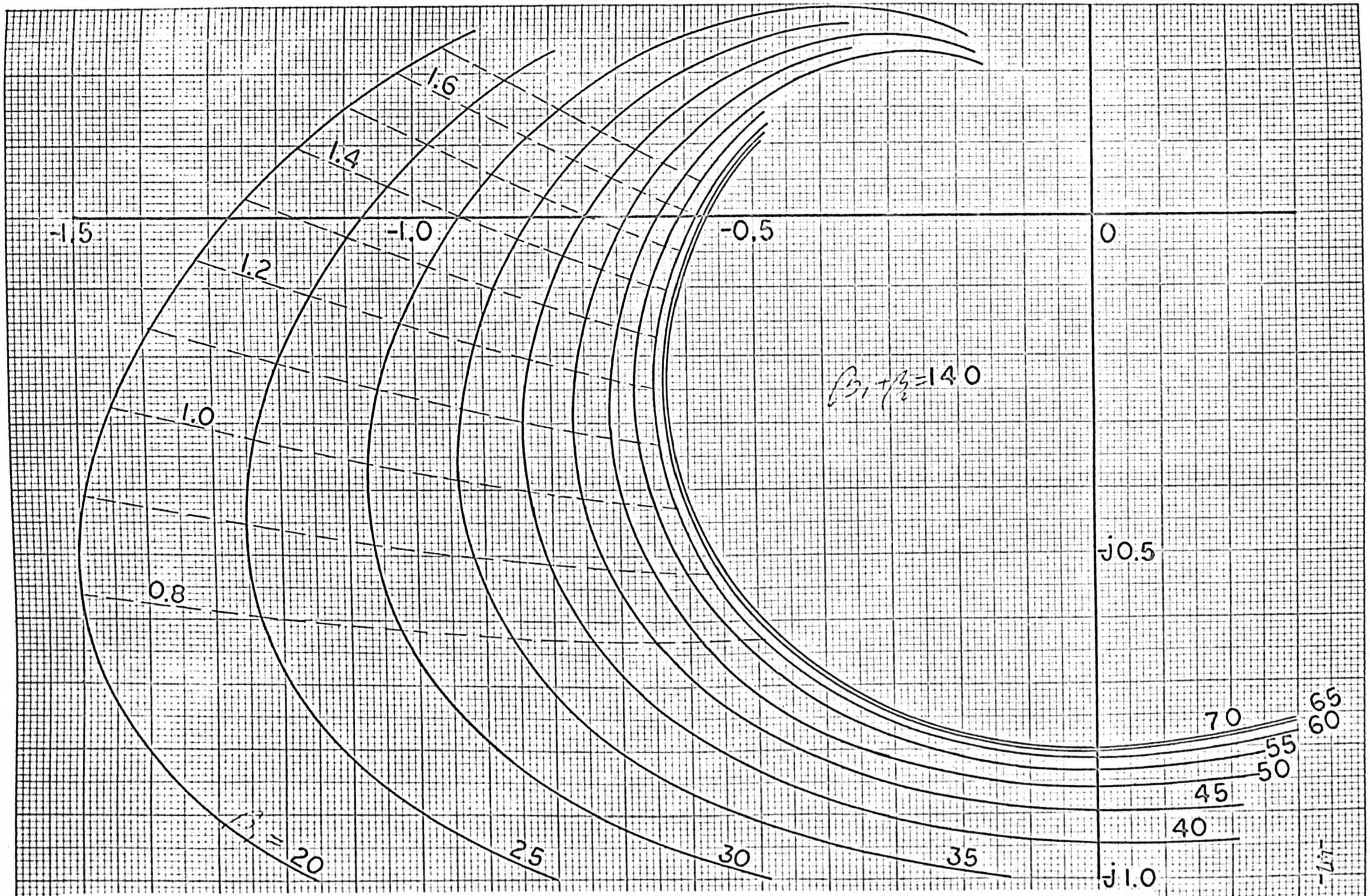

Fig. 37 Modified frequendy response loci for on-off with dead-zone and $G(s)=\frac{1-sT}{(1+sT)^2}$

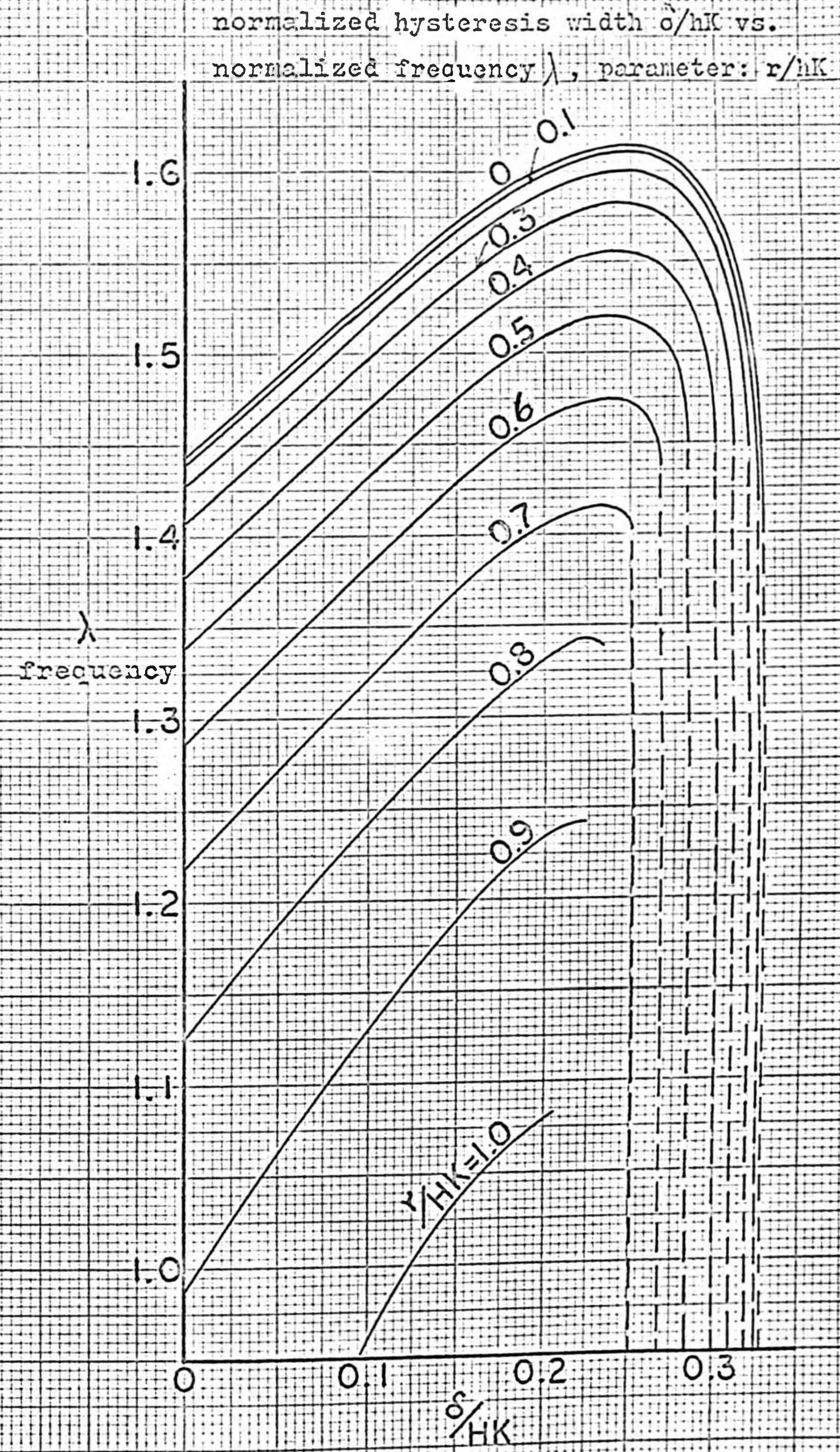

Fig. 38 Oscillating frequency of the system with on-off with dead-zone and $G(s)=\frac{K(1-sT)}{(1+sT)^2}$

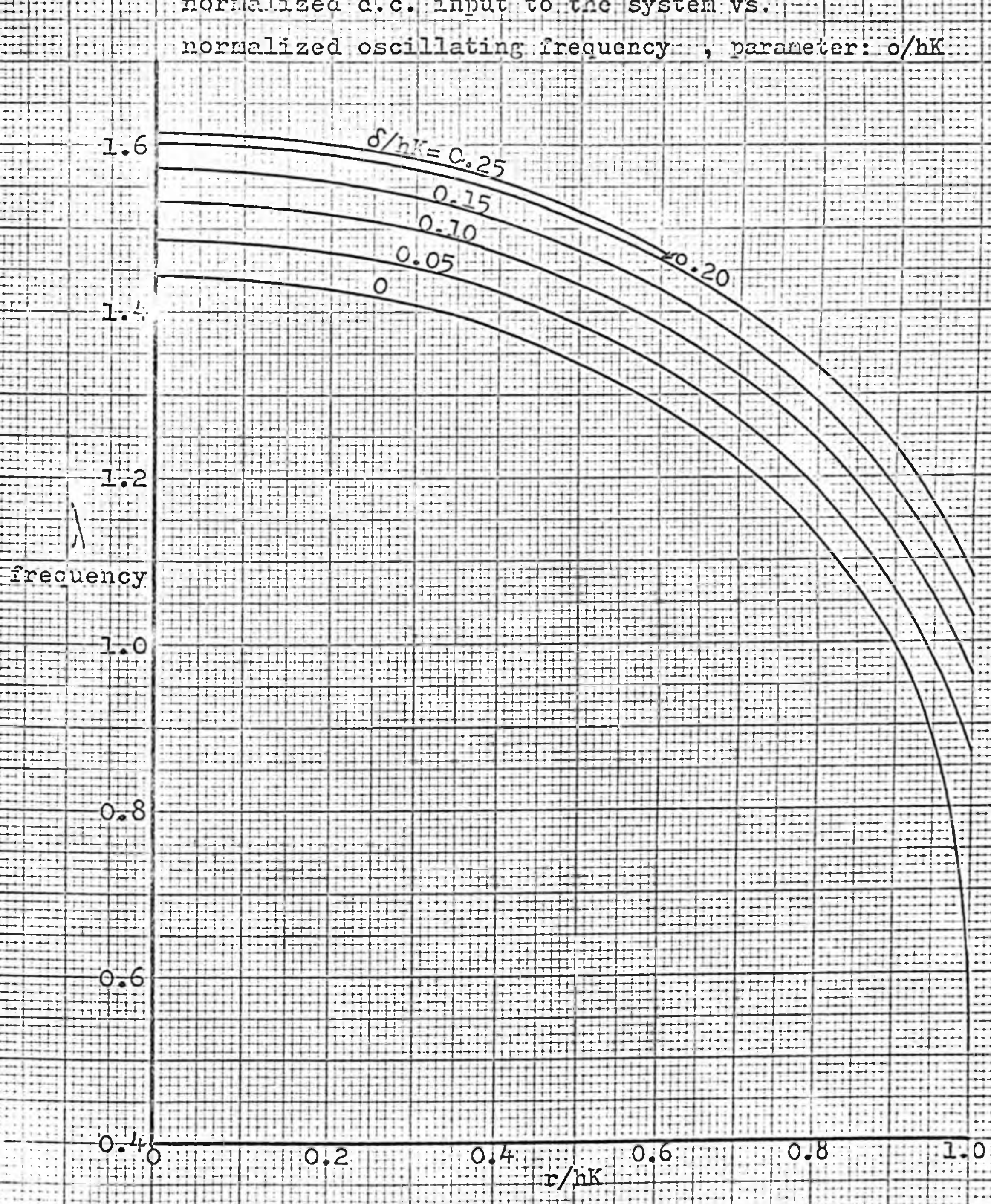

Fig. 39 Oscillating frequency of the system with on-off with dead-zone and $G(s)=\dfrac{K(1-sT)}{(1+sT)^2}$

Comparisons between experimental and the theoretical results are shown in fig. 40 for the three cases (a) no d.c. input, (b) a constant r/hK and (c) a constant δ/hK, with good agreement.

It should be noted that the system has at least three modes of stable state, namely (a) no oscillation, (b) normal oscillation and (c) limping oscillation. When the system's d.c. input has a smaller value than dead-zone δ, it is necessary to give an initial excitement to start the oscillation. When the d.c. input is comparatively greater than the dead-zone value δ, there is a possibility of limping oscillation in which the output of the non-linearity takes only two values, zero and either +h or -h (depending on the polarity of d.c. input). The change from the normal oscillation mode to the limping oscillation mode and vice versa has a hysteresis effect with this particular linear transfer function.

The boundaries of the change of mode may be determined by the following procedure:(assuming the d.c. input is positive,) (1) evaluate the possible oscillating frequency in terms of δ/hK for normal and limping mode, (2) calculate the positive peak amplitude of the system output waveform at the frequency for both mode, then (3) find the system constants δ/hK and r/hK when the difference of the d.c. input and the peak value of the output signal (feedback signal) becomes equal to δ. This can be done graphically or by the use of a digital computer. For the analysis of the possible limping oscillation mode, the system can be assumed as a pure on-off having the output heights of ±h/2, with a d.c.

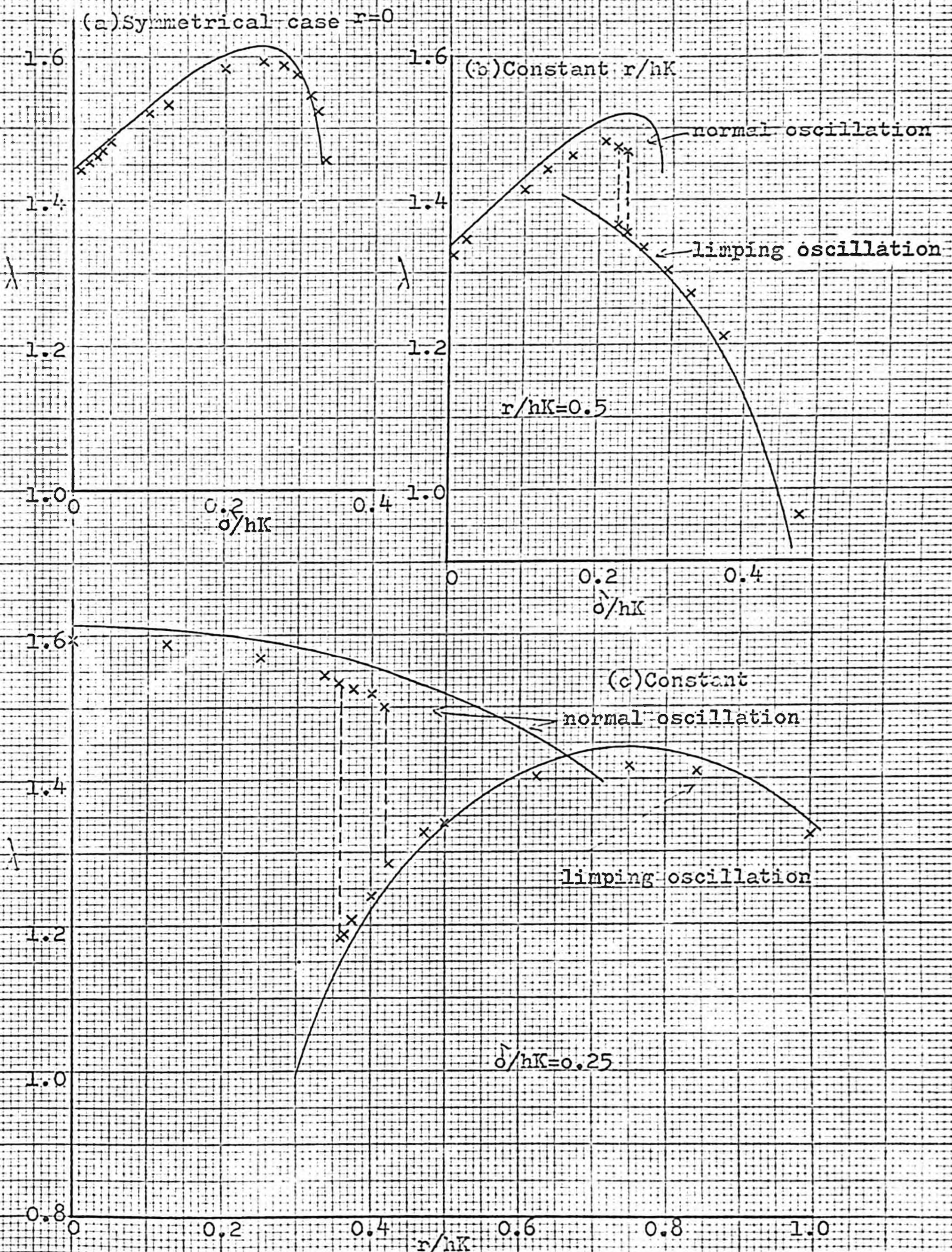

Fig. 40 Experimental results by simulation

input to the system $r-\delta$, and with an extra d.c. input h/2 to the output of the non-linearity. In this particular case, the actual calculation for the limping oscillation was done using the solution of r/hK in terms of λ (from fig. 39), then substituted this value (r/hK) to $(r-\delta)hK - 1/2$ in which r, δ, h and K are the actual system constants.

3.5 Saturation and $G(s) = \dfrac{K(1 - sT)}{(1 + sT)^2}$

The basic scheme of fig. 24 is again considered with the non-linear element, a saturation* characteristic, r equal to zero. For this symmetrical case, using eqns. 147 and 148, the modified frequency response is

$$\mathrm{Re}\left[A(j\lambda)\right]_{\beta} = \sum_{n=1}^{\infty} \frac{a_n \cos n\beta}{a_1 \cos\beta} \mathrm{Re}\left[G(jn\omega)\right] \qquad 187$$

$$\mathrm{Im}\left[A(j\lambda)\right]_{\beta} = \sum_{n=1}^{\infty} \frac{a_n \sin n\beta}{a_1 \sin\beta} \mathrm{Im}\left[G(jn\omega)\right] \qquad 188$$

where $\lambda = \omega T$ and n is odd only.

Rewriting above expressions by taking a new angle $\chi = \frac{\pi}{2} - \beta$ 189

$$\mathrm{Re}\left[A(j\lambda)\right]_{\chi} = \sum_{n=1}^{\infty} \frac{a_n \sin n\chi \sin(n\pi/2)}{a_1 \sin\chi} \mathrm{Re}\left[G(jn\omega)\right] \qquad 190$$

$$\mathrm{Im}\left[A(j\lambda)\right]_{\chi} = \sum_{n=1}^{\infty} \frac{a_n \cos n\chi \sin(n\pi/2)}{a_1 \cos\chi} \mathrm{Im}\left[G(jn\omega)\right] \qquad 191$$

The Fourier coefficient a_n's are found to be

$$a_n = \frac{2h}{n\pi} \frac{\sin(n\pi/2)}{\sin\chi} \left[\frac{\sin(n+1)\chi}{n+1} + \frac{\sin(n-1)\chi}{n-1} \right] \qquad 192$$

and again the linear transfer function, transfering the gain K to the non-linear part, is

$$G(jn\omega) = \frac{1-3n^2\lambda^2}{(1+n^2\lambda^2)^2} + j\frac{(n^2\lambda^2-3)n\lambda}{(1+n^2\lambda^2)^2} .$$

* We assume that the slope of this saturation characteristic is unity. For other values of slope the value K in eqns. 195 and 196 is replaced by K (slope of the saturation).

Hence,

$$Re\left[A(j\lambda)\right]_{\alpha} = \frac{\sum_{n=1\ odd}^{\infty} \frac{\sin n\alpha}{n} \frac{\sin(n+1)\alpha}{n+1} \frac{\sin(n-1)\alpha}{n-1} \frac{1-3n^2\lambda^2}{(1+n^2\lambda^2)^2}}{\sin\alpha\ (\alpha + \frac{\sin 2\alpha}{2})} \qquad 193$$

$$Im\left[A(j\lambda)\right]_{\alpha} = \frac{\sum_{n=1odd}^{\infty} \cos n\alpha \frac{\sin(n+1)\alpha}{n+1} \frac{\sin(n-1)\alpha}{n-1} \frac{(n^2\lambda^2-3)}{(1+n^2\lambda^2)^2}}{\cos\alpha\ (\alpha + \frac{\sin 2\alpha}{2})} \qquad 194$$

While the critical function for the saturation characteristic is given by

$$C\ (\alpha) = -\frac{\pi}{K(2\alpha + \sin 2\alpha)} \qquad 195$$

When the system oscillates, the relationship between gain K and the normalized frequency λ will be obtained from the relationship

$$\frac{1}{K} = -\frac{1}{\pi}(2\alpha + \sin 2\alpha) Re\left[A(j\lambda)\right]_{\alpha, I_m[A]=0} \qquad 196$$

The modified frequency response loci $\left[A\ (j\lambda)\right]_{\alpha}$, evaluated by the digital computer, as a function of λ for several values of α and the describing function for satulation are shown in fig. 42 and 43. From these loci the variation of the frequency of oscillation with the d.c. loop gain K was determined and compared with the experimental data and results using the normal decribing functions, as shown in fig. 44.

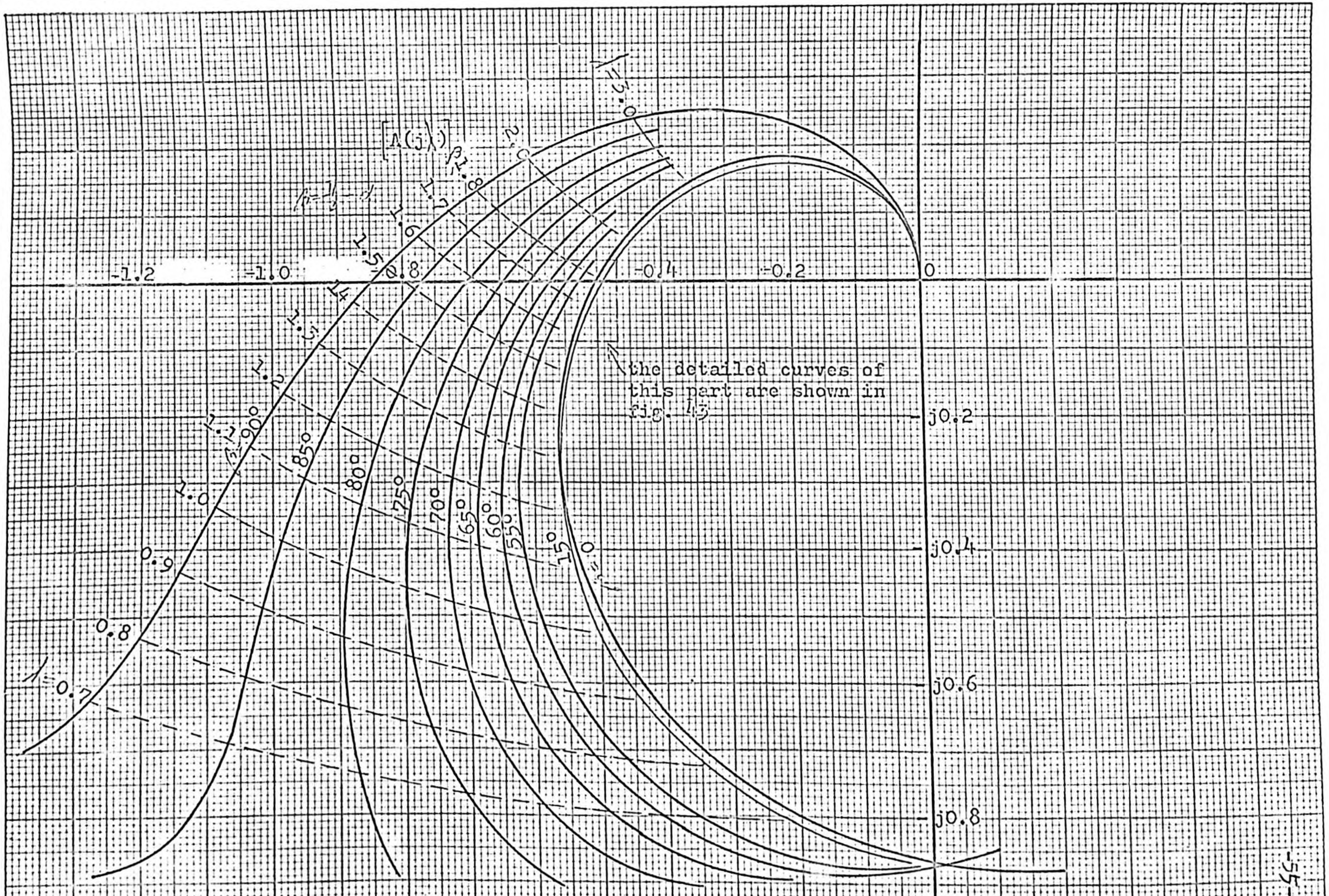

Fig. 42 Modified frequency response loci for saturation and $G(s) = \frac{1 - sT}{(1+sT)^2}$

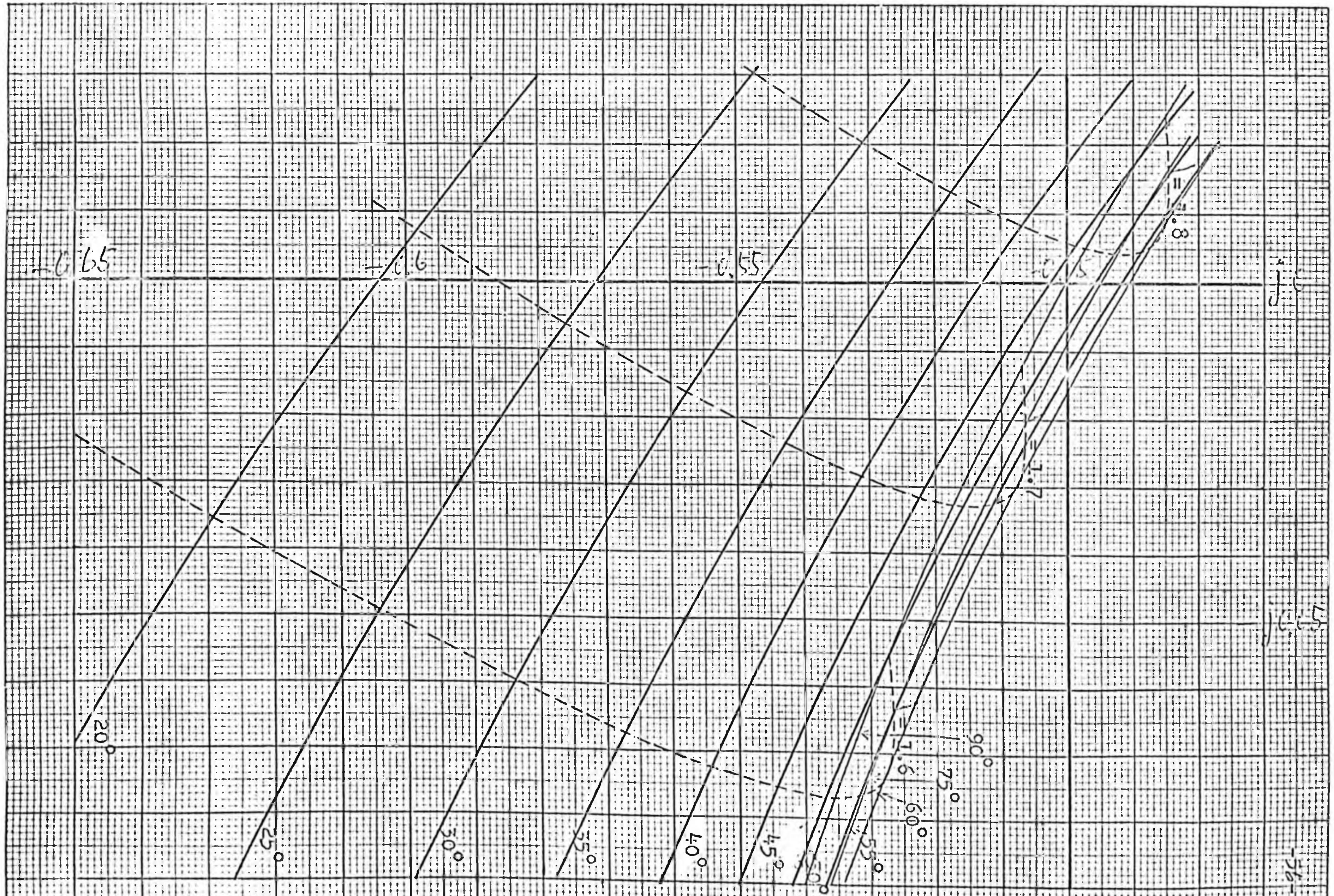

Fig. 43 Detail of modified frequencyrresponse loci for saturation and $G(s)=(1-sT)/(1+sT)^2$

Fig. 44 Theoretical results and [illegible] results for [illegible] and $F(\cdot) = (1-[illegible])/(1+[illegible])^2$

Looking at the graph we see that the theoretical result is not satisfactory except when the gain K is fairly large. The theory gives a big error (max. 5%) when the system works at a slight clipping level. It is worse here than that obtained by the ordinary describing function technique. The main reason for this is the fact that the waveform of the input to the non-linearity becomes distorted and the resultant output has a shape which should not be assumed to be a clipped sinusoidal as shown in fig. 45. Therefore, it seems that the Fourier coefficient a_n might be compensated by some means.

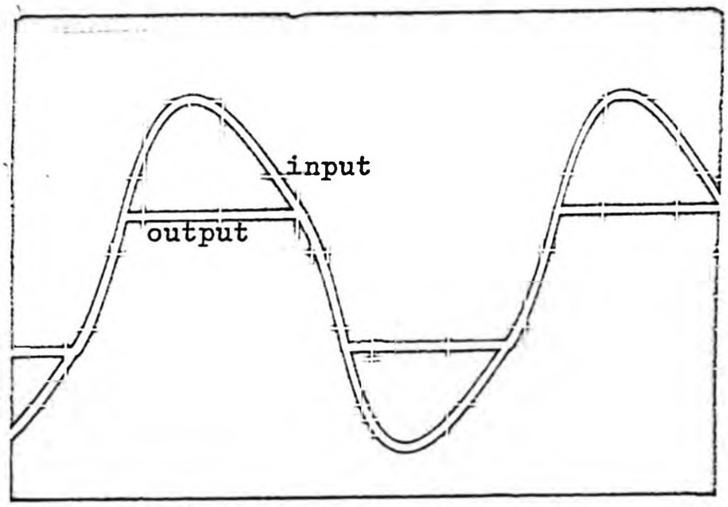

Fig. 45 Input and output waveforms of the saturation in a closed loop system; $G(s)=\frac{K(1-sT)}{(1+sT)^2}$

3.6 Experimental Procedure

3.6.1 Measurement circuits

Fig. 51 shows the standard form of the setup which simulate the non-linear systems discussed in the theory. One input to the amp.1 (marked "A") corresponds to the system input, and an external d.c. signal is applied to it. The output of amp.6 (marked "B") correspondes to the system output and is fed back to amp.1. Amp.2 is an unity gain inverter to be used when the non-linearity is of the out-of-phase type (output goes positive when input goes negative. Dead-zone and on-off systems are of this type. Amp.2 is by-passed by SW_1 when the non-linearity is of the in-phase type (saturation). To compensate for assymmetry of the non-linearity, two adjustable d.c. voltages E_1 and E_2 are provided at the inputs to amp.1 and amp.3. Amps. 8, 4 and 5 simulate the transfer function $\frac{1-sT}{(1+sT)^2}$ or $\frac{1}{1+sT}$ depending on the position of SW_2. With SW_2 in the "upper" position, the transfer ratio is

$$\left(1+\frac{-2}{1+sT}\right)\left(\frac{-1}{1+sT}\right) = \frac{1-sT}{(1+sT)^2}$$

and with SW_2 in the "down" position (thereby omitting amp.4) it is $\frac{-1}{1+sT}$. The variable gain K is obtained using amp.6 which gives min. and max. gains of 1/6 and 6 in this case. When higher gain is required, the two 100 kilohm resisters in the amp.6 are changed to other appropriate values. The 500k potentiometer in amp.6 is calibrated.

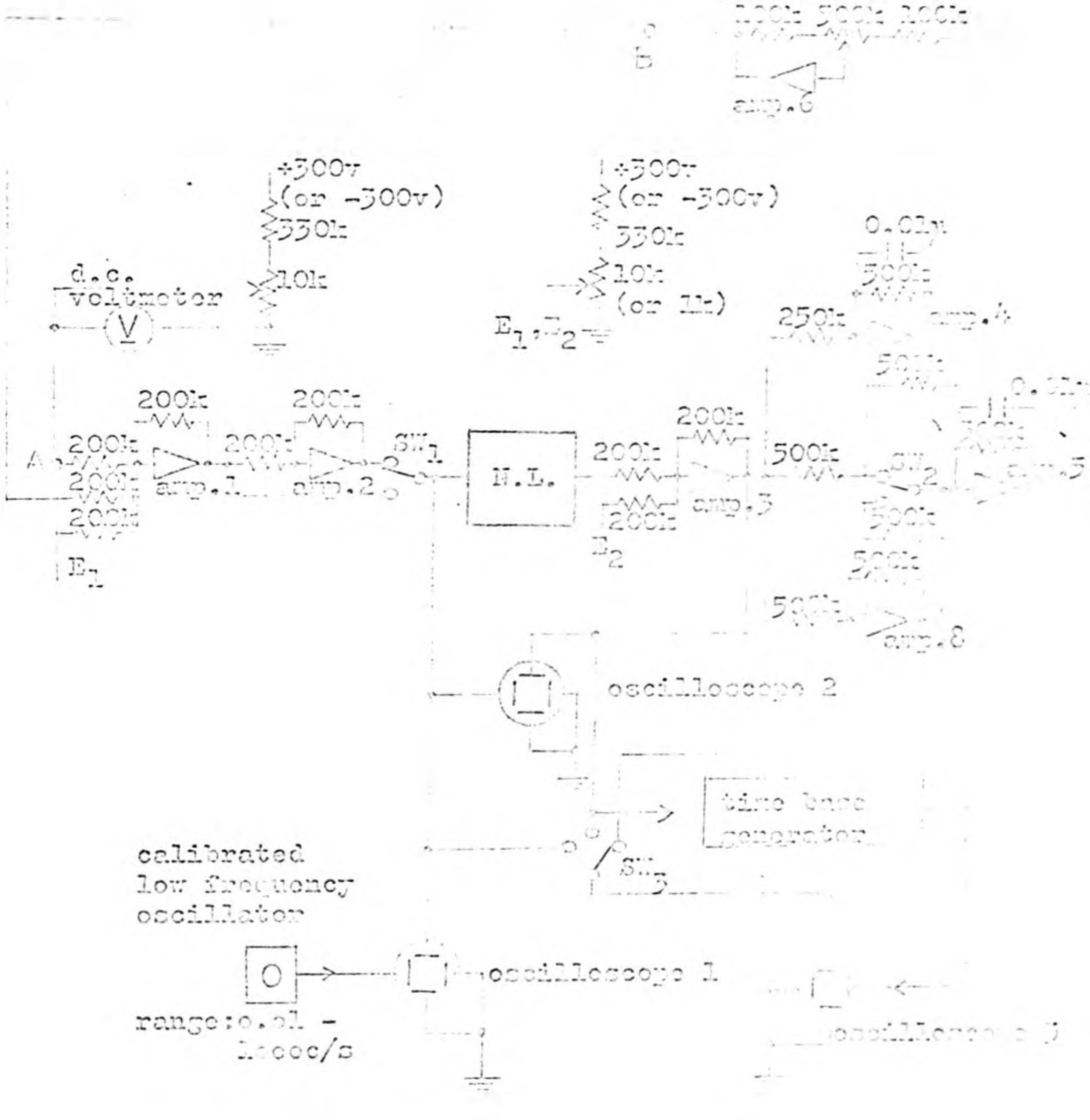

Fig. 51 Standard setup of non-linear system simulation.

Oscilloscope 1 is used for the measurement of frequency of oscillation by comparison with a signal generator as a standard of frequency. Oscilloscopes 2 and 3 are helpful for the initial balancing of the operational amplifiers and the non-linear characteristic, and also for observing the variation of waveforms during measurements. The former gives direct indication of the input and output characteristic of the non-linearity and the latter is used to observe waveforms at various other points in the system.

3.6.2 Procedure

After leaving the system in a normal operation state for at least 5 hours to avoid initial drifts, each unit amplifier in the system is balanced by adjusting the positive bias to the positive input, and the non-linear characteristic using E_1 and E_2.

Then the gain K and d.c. input voltage r are changed in appropriate steps and measured on the calibrated dial of the potentiometer in amp. 6 and by the d.c. voltmeter. The corresponding oscillating frequency at each step (if present) is measured on the dial of the low frequency oscillator which is adjusted to give a still Lissajous pattern on oscilloscope 1.

The non-linear constants (δ, h) are measured by oscilloscope 2 (calibrated) when the system is in operation

REFERENCES

(1) JOHNSON, C. L.:"Analog Computer Techniques", Second Edition 1963, McGraw-Hill, N.Y.

(2) FIFER, S.:"Analog Computation" 1961, McGraw-Hill, N.Y.

(3) Philbrick, "Application Manual for Philbrick Computing Amplifiers", George A, Philbrick Researches, Inc., Boston, Mss, U.S.A.

(4) Denki Tsushin Gakkai, "Modern Pulse Technique", The Communication Society of Japan, 1962, Corona Pub. Inc., Japan.

(5) GILL, J. C., PELEGRIN, M. J. AND DECAULNE, P.:"Feedback Control Systems", McGraw-Hill, N.Y., 1959.

(6) THALER, G. J. and PASTEL, M. P.:"Analysis and Design of Non-Linear Feedback Control System", McGraw-Hill, N.Y., 1962.

(7) JOLLEY, L. B. W.:"Summation of Series Collected by L. B. W. Jolley", Second Revised Edition, 1961, Dover Publications Inc., New York.

APPENDIX I CRITICAL LOCUS FUNCTION

(1) On-Off with Hysteresis

(a) Symmetrical Case: $$c = -\frac{\pi\sqrt{a^2-\delta^2}}{4h} - j\frac{\pi\delta}{4h}$$

(b) Assymmetrical Case: $$C = \frac{\pi r_i}{2h\ \sin 2\beta} - j\frac{\pi\delta}{4h\ \sin^2\beta}$$

(2) On-Off with Dead-Zone

(a) Symmetrical: $$C = \frac{\delta}{2h\ \sin 2\beta}$$

(b) Assymmetricl: $$C = -\frac{\pi\delta}{h(\cos\beta_1 + \cos\beta_2)(\sin\beta_1 + \sin\beta_2)}$$

(3) On-Off with Dead-Zone and Hysteresis, Symmetrical Case :

$$C = -\frac{(2\delta + \Delta)}{4h\ \sin 2\beta} - j\frac{-\pi\Delta}{8h\ \sin^2\beta}$$

(4) Saturation

(a) Symmetrical: $$C = -\frac{\pi\delta}{h(2\alpha + \sin 2\alpha)}$$

(b) Assymmtrical: $$C = -\frac{\pi\delta}{h\left[\sin(\beta_1+\beta_2) - \beta_1 - \beta_2 + 2(\cos^2\beta_2 - \cos^2\beta_1) \times (\sin\beta_2 - \sin\beta_1) + \pi\right]}$$

APPENDIX II SUMMATION OF INFINITE SERIES

(1) Cosine Series: $$C_{j,k}(\lambda,\alpha) = \sum_{n=1}^{\infty} \frac{n^j \cos n\alpha}{(1+n^2\lambda^2)^k}$$

$$C_{0,1} = \frac{\pi}{2\lambda \sinh \pi/\lambda} \cosh \frac{\pi-\alpha}{\lambda} - \frac{1}{2}$$

$$C_{0,2} = \frac{\pi}{4\lambda \sinh \pi/\lambda}\left[\cosh\frac{\pi-\alpha}{\lambda} + \frac{\alpha}{\lambda}\sinh\frac{\pi-\alpha}{\lambda} + \frac{\pi\cosh \alpha/\lambda}{\lambda \sinh \pi/\lambda}\right] - \frac{1}{2}$$

$$C_{2,2} = \frac{\pi}{4\lambda^3 \sinh \pi/\lambda}\left[\cosh\frac{\pi-\alpha}{\lambda} - \frac{\alpha}{\lambda}\sinh\frac{\pi-\alpha}{\lambda} - \frac{\pi\cosh \alpha/\lambda}{\lambda \sinh \pi/\lambda}\right]$$

$$C_{4,3} = \frac{\pi}{16\lambda^7 \sinh^3(\pi/\lambda)}\Bigg[-\lambda^2 \sinh\frac{\pi}{\lambda}\Bigg\{\sinh\frac{\pi}{\lambda}\cosh\frac{\pi-\alpha}{\lambda} - \frac{\pi}{\lambda}\cosh\frac{\alpha}{\lambda} + \frac{\alpha}{\lambda}\sinh\frac{\pi}{\lambda}\sinh\frac{\pi-\alpha}{\lambda}$$

$$+ \frac{\pi\alpha}{\lambda^2}\left(\sinh\frac{2\pi-\alpha}{\lambda} + \cosh\frac{\alpha}{\lambda}\right) - \frac{\alpha^2}{\lambda^2}\sinh\frac{\alpha}{\lambda}\cosh\frac{\pi-\alpha}{\lambda}\Bigg\} + \left(4\lambda\sinh\frac{\pi}{\lambda} - 2\pi\cosh\frac{\pi}{\lambda}\right)$$

$$\left(\lambda\sinh\frac{\pi}{\lambda}\cosh\frac{\pi-\alpha}{\lambda} - \alpha\sinh\frac{\pi}{\lambda}\sinh\frac{\pi-\alpha}{\lambda} - \pi\cosh\frac{\alpha}{\lambda}\right)\Bigg]$$

$$C_{0,3} = C_{0,1} - 2\lambda^2 C_{2,2} + \lambda^4 C_{4,3}$$

$$C_{2,3} = C_{2,2} - \lambda^2 C_{4,3}$$

See reference (7), page 104.

(2) Sine Series: $$S_{j,k} = \sum_{n=1}^{\infty} \frac{n^j \sin n\alpha}{(1+n^2\lambda^2)^k}$$

$$S_{-1,1} = \frac{\pi}{2}\left[1 - \frac{\sinh\frac{\pi-\alpha}{\lambda}}{\sinh\frac{\pi}{\lambda}}\right] - \frac{\alpha}{2}$$

$$S_{1,1} = \frac{\pi}{2\lambda^2}\frac{\sinh\frac{\pi-\alpha}{\lambda}}{\sinh\frac{\pi}{\lambda}}$$

$$S_{1,2} = \frac{\pi}{4\lambda^3 \sinh^2(\frac{\pi}{\lambda})}\left(\alpha\cosh\frac{\pi-\alpha}{\lambda}\sinh\frac{\pi}{\lambda} - \pi\sinh\frac{\alpha}{\lambda}\right)$$

$$S_{-1,1} = S_{-1,1} - \lambda^2 S_{1,2}$$

$$S_{3,3} = \frac{\pi}{16\lambda^6\sinh^3(\frac{\pi}{\lambda})}(3\lambda\sinh\frac{\pi}{\lambda} - 2\pi\cosh\frac{\pi}{\lambda})(\alpha\cosh\frac{\pi-\alpha}{\lambda}\sinh\frac{\pi}{\lambda} - \pi\sinh\frac{\alpha}{\lambda})$$

$$+ \sinh\frac{\pi}{\lambda}(\alpha\pi\cosh\frac{2\pi-\alpha}{\lambda} - \pi\lambda\cosh\frac{\alpha}{\lambda} - \alpha^2\sinh\frac{\pi}{\lambda}\sinh\frac{\pi-\alpha}{\lambda})$$

$$S_{1,3} = S_{1,2} - \lambda^2 S_{3,3}$$

$$S_{-1,3} = S_{-1,1} - 2\lambda^2 S_{1,2} + \lambda^4 S_{3,3}$$

See reference (7), page 104.

APPENDIX III FOURIER COEFFICIENT OF PERIODIC WAVEFORMS

(1) Output of On-Off with Hysteresis

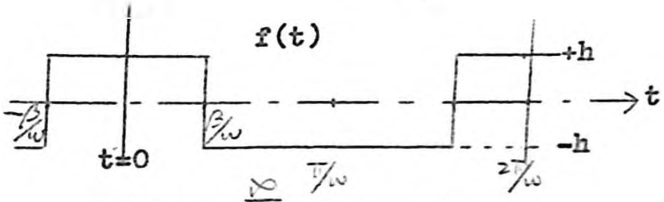

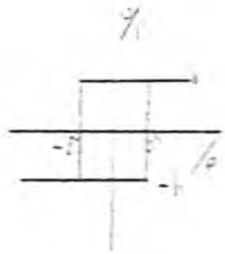

$$f(t) = \sum_{n=1}^{\infty} a_n \cos n\omega t$$

$$a_n = \frac{4h}{n\pi} \sin n\beta \qquad n \geq 1$$

$$a_o = \frac{2h}{\pi}\left(\beta - \frac{\pi}{2}\right)$$

(2) Output of On-Off with Dead-Zone

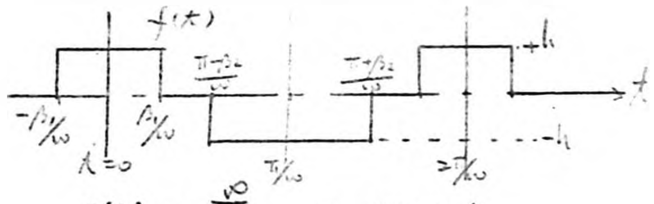

$$f(t) = \sum_{n=1}^{\infty} a_n \cos n\omega t$$

$$a_n = \frac{2h}{n\pi}(\sin n\beta_1 - \cos n\pi \sin n\beta_2)$$

$$a_o = \frac{h}{\pi}(\beta_1 - \beta_2)$$

(3) Output of Saturation (input: sinusoidal)

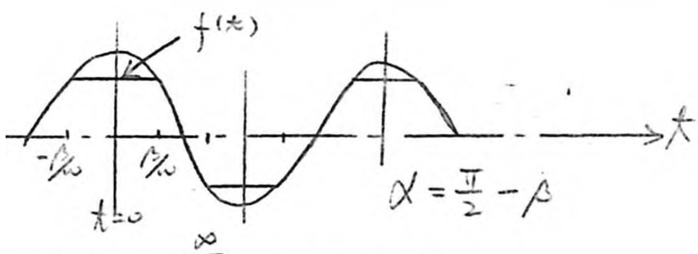

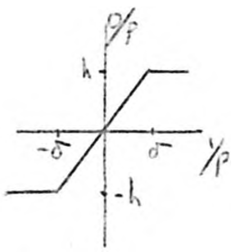

$$f(t) = \sum_{n=1}^{\infty} a_n \cos n\omega t$$

$$a_n = \frac{2h \sin(n\pi/2)}{n\pi \sin\alpha}\left[\frac{\sin((n+1)\alpha)}{n+1} + \frac{\sin((n-1)\alpha)}{n-1}\right]$$

$$a_o = 0$$